Université de Montréal

New functional polymer resins with pore size specificity

par

Mu Yang

Département de chimie

Faculté des arts et des sciences

Mémoire présenté à la Faculté des études supérieures

en vue de l'obtention du grade de

Maître ès sciences (M.Sc.)

en chimie

Avril 1999

Université de Montréal

Faculté des études supérieures

Ce mémoire intitulé

New functional polymer resins with pore size specificity

présenté par:

Mu Yang

a été évalué par un jury composé des personnes suivantes:

Michel Lafleur	président-rapporteur
Julian Zhu	directeur de recherche
François Brisse	membre du jury

Mémoire accepté le: 99.06.23

Abstract

New functional polymer resins with pore size and shape specificity were prepared by the use of micellar template imprinting technique. We have made several series of porous polymer resins based on styrene-divinylbenzene and methyl methacrylate-ethylene glycol dimethacrylate. Sodium *bis*(2-ethylhexyl) sulfosuccinate (AOT) is a surfactant capable of forming reverse micelles and solubilizing large amounts of water. The pore size of the polymers was controlled by varying the amount of water in the AOT reverse micelles. Polymerizable cosurfactants were also used to introduce functional groups into the pores by the formation of mixed micelles. To improve the accessibility of the pores, toluene was used as the pore-forming reagent in the preparation of the resins.

The chemical compositions of the polymer resins and the presence of the functional groups were confirmed by solid state nuclear magnetic resonance and infrared spectroscopy. BET gas adsorption was employed to examine the surface area and pore size of polymer resins. The porous polymer resins with poly(methyl methacrylate) matrix were compared with those based on polystyrene matrix. The results are similar, the pore size changed gently by varying water content in reverse micelles. The addition of pore-forming reagents improved the specific surface area of the resins and hence the accessibility of the pores.

We tested the selective binding of metal cations such as Ca(II) and Ni(II) by the functional porous polymer resins. The kinetics of binding and the effects of cation concentration and of the pH of the solution were also studied. The polymer resin can be used as stationary phase in chromatographic columns for the separation of cations.

Sommaire

De nouvelles résines polymères ont été préparées par la méthode des empreintes micellaires. Ainsi, plusieurs séries d'échantillons à matrices styrène-divinylbenzene ou méthacrylate de méthyle-diméthacrylate d'éthylène glycol ont été synthétisées, dont la particularité réside dans la taille de pores contrôlée et la fonctionalisation. Le *bis*(2-éthylhexyl) sulfosuccinate de sodium (AOT) a été utilisé comme surfactant, compte tenu de sa capacité de former des micelles inverses et de solubiliser de grandes quantités d'eau. La taille des pores, a dès lors, été ajustée en variant la quantité d'eau dissoute dans les micelles inverses d'AOT. D'autre part, des groupements fonctionnels ont été introduits dans les pores par l'intermédiaire de co-surfactants polymérisables participant à la formation des micelles. Afin d'améliorer l'accessibilité des cavités créees dans certaines matrices, le toluène a été utilisé comme générateur de canaux d'accès.

Les résines polymères ont été caractérisées par différentes méthodes physico-chimiques. Leur composition chimique a été déterminée par spectroscopie de résonance magnétique nucléaire du ^{13}C à l'état du solide et par spectroscopie infrarouge. L'adsorption gazeuze de BET a permis d'évaluer l'aire de la surface poreuse ainsi que la taille des pores. Une comparaison a été établie entre les deux types de résines, respectivement, celles à matrice styrène-divinylbenzène et celles à matrice méthacrylate de méthyle-diméthacrylate d'éthylène glycol. Les résultats sont globalement semblables, la taille de pore varie graguellement avec la teneur en eau des micelles inverses. D'autre part, l'addition d'un générateur de pores s'est révélée efficace quant à l'augmentation de l'aire de la surface

poreuse, c'est à dire en fait, de l'accessibilité des cavités créées par les empreintes micellaires.

En dernier lieu, nous avons testé l'adsorption sélective de cations métalliques tels que Ni(II) et Ca(II) par nos résines poreuses fonctionalisées. La cinétique d'adsorption, les effets de la concentration des cations et du pH des solutions d'ions métalliques ont été étudiés. Il en ressort que nos résines poreuses fonctionalisées semblent prometteuses pour un usage comme phase stationnaire en chromatographie par échange d'ions.

Table of Contents

List of Figures

List of Tables

List of Abbreviations and Symbols

Å	Angström
AIBN	2,2'-azoisobutyronitrile
AOT	Sodium *bis*(2-ethy-1-1hexyl) sulfosuccinate
BET	Brunauer, Emmet and Teller
BJH	Barret, Joyner and Halanda
c	BET constant
D	Pore diameter
D_{av}	Average pore diameter
D_{mv}	The diameter with maximal volume increment
DBK	Dibenzyl ketone
DCM	Dichloromethane
DVB	Divinylbenzene
EGDMA	Ethylene glycol dimethacrylate
h	Hour
HEMA	2-hydroxyethyle methacrylate
HPLC	High performance liquid chromatography
IR	Infrared
IUPAC	International Union of Pure and Applied Chemistry
kJ	KiloJoule
min	Minute
MMA	Methyl methacrylate

mol	Mole
M_V	Molar volume
N	Avogadro number
Na11-EAAU	Sodium 11-(N-ethylacrylamido) undecanoate
nm	Nanometer
NMR	Nuclear magnetic resonance
Ⓟ	Polymer
P	Pressure
PS	Polystyrene
ppm	mg/L
PMMA	Poly(methyl methacrylate)
R	Gas constant (R = 0.082)
r_c	core radius
r_P	Cylindrical pore radius
S	Styrene
SANS	Small-angle neutron scattering
S_{BET}	BET specific surface area
SDS	Sodium dodecylsulfate
SEC	Size exclusion chromatography
T	Temperature
t	Adsorbate layer thickness
THF	Tetrahydrofuran
TLC	Thin layer chromatography

TSAs	Transition state analogues
V_m	Monolayer volume capacity
W	Molar ratio $[H_2O]/[AOT]$
γ	Tension of liquid surface
σ	Area occupied by one adsorbate molecule
μm	Micrometer

Acknowledgement

First of all, I would like to express my sincere gratitude to my research director, Professor Julian Zhu, for his continuous encouragement, advice and guidance on both research and life.

I would also like to thank Environmental Science and Technology Alliance Canada (ESTAC) and Natural Science and Engineering Research Council (NSERC) of Canada for their financial support.

I wish to thank all my colleagues in this group for their friendship, helpful discussion and continuous support. Special thanks go to Dr. Huiyou Liu, who gave a lot of advices on organic synthesis, Mr. Laurent Masaro, who helped with the characterization with solid state NMR spectroscopy, and Dr. Mohand Ousalem, for his precious help during the writing of this thesis.

Finally, the assistance of all members of the chemistry department of Université de Montréal is gratefully acknowledged.

1. Introduction

The polymer resins with pore size specificity have already found applications in selective catalysis of a chemical reaction, separation of compounds closely related in structure and properties, and adsorption and exchange of specific anions or cations. The principle of size exclusion has long been used in the fractionation of macromolecules of different molecular weights [1]. The size and shape of the molecules or molecular aggregates can play important roles in chemical and biochemical processes [2,3]. The template-imprinting techniques have been used to prepare polymer resins with size and shape specificity.

These polymer resins can be use as stationary phase in chromatographic separation such as size exclusion chromatography (SEC) and high performance liquid chromatography (HPLC). The presence of cavities with pre-defined size and shape is one of the most important characteristics of these polymer resins.

In our laboratory, we have used reverse micelles as imprinting templates in the preparation of crosslinked porous polymer resins, using styrene-divinylbenzene and methyl methacrylate-ethylene glycol dimethacrylate as the polymer matrices and sodium *bis*(2-ethylhexyl sulfosuccinate (AOT) as the surfactant. The pore size of the polymers was controlled by varying the amount of water in the AOT reverse micelles. Polymerizable cosurfactants were also used to introduce functional groups to polymer resins.

1.1 Template-Imprinted Polymers

1.1.1 Template-imprinting techniques

During the past years, template-imprinting techniques have drawn much research attention, because it was found to be an effective means of producing polymers exhibiting molecular recognition properties [4-6], which play important roles in biological activity of enzymes, receptors or antibodies. Progress has been made by incorporating the specific binding sites in the crosslinked polymer matrix obtained by copolymerization with the template molecules. These materials are called template-imprinted polymer resins. As shown in Figure 1.1, template molecules are dissolved in a mixture of monomers and crosslinkers prior to their polymerization. The templates may contain functional groups and double bonds as polymerizable groups. Once the polymerization is completed, these template molecules can be removed by a simple extraction or a combined chemical hydrolysis and extraction so that the polymer is left with imprints of the original templates.

The pioneer work on template-imprinting techniques was performed by Dickey and Curti in 1950 [7,8]. They carried out the first analogue synthesis of antibodies by the polymerization of a solution of silicate in the presence of an organic coloring agent. Some 20 years later, in 1972, Wulff and Sarhan prepared analogue polymers of enzymes with this technique [9]. They used D-glyceric acid as the template and the two monomers used were *p*-vinylphenylboron acid and *p*-vinylaniline.

Generally, the template-imprinted polymers were macroporous materials with a high internal surface area (250-500 m^2/g) and a large pore diameter (50 nm), so that small molecules of solvents or reagents can have access to the cavities [10,11]. The templates are surrounded by the monomer units with or without functional groups. The interactions or linkages can be covalent bonds or weak intermolecular forces such as electrostatic forces,

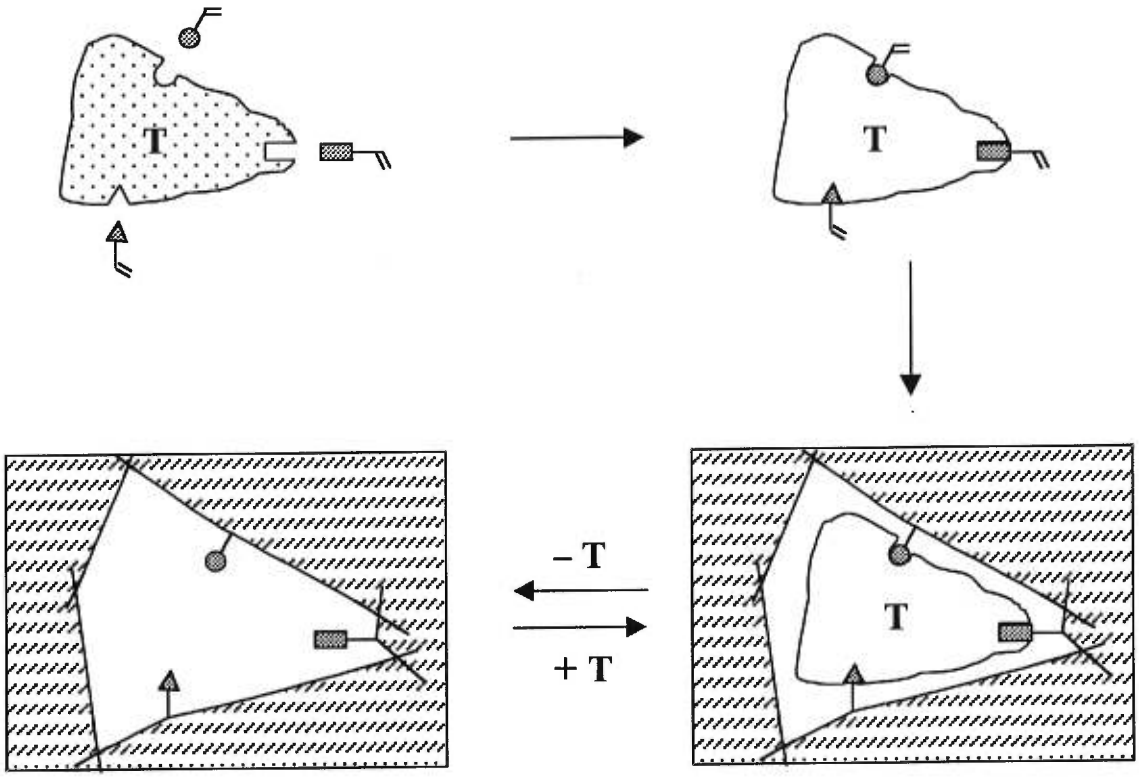

Figure 1.1 The preparation of a polymer resin with the template-imprinting techniques. The specific size and shape of functional cavities in the polymer resin can be controlled by the use of templates.

hydrogen bonds or hydrophobic interactions [11]. The polymerization was done in bulk, or in suspension or dispersion systems. Dispersion polymerization is defined as a modified precipitation polymerization where the monomer but not the polymer is soluble in the dispersion medium and where well-defined polymer particles are formed [12,13].

The structure of polymer matrix is important to these template-imprinted materials. To obtain useful polymer resins of this kind, the following conditions are required [10]:

1. Rigidity to maintain the shape of the cavity after the removal of templates,
2. Flexibility of the backbone to reach an equilibrium rapidly,
3. Accessibility of the cavities for the targeted guest molecules,
4. Good mechanical stability for applications under high pressures (such as HPLC) or as catalysts in stirred reactors,
5. Good thermostability for applications at high temperatures.

1.1.2 Applications of template-imprinted polymers

Many applications have been found for template-imprinted polymers, in separation and isolation [14,15], as antibody and receptor mimics in immunoassay-type analyses [16-18], as enzyme mimics in catalytic applications [19], and in biosensor-like devices [20-22].

Ion-exchange resins prepared with template-imprinting techniques can be used for the removal and concentration of metal cations, and fractionation of polyelectrolytes. They can be useful in processes such as deionization, demineralization, dealkalination and desilicazation. Zwiterionic resins or combinations of ion-exchange resins can completely remove specific electrolytes. Dilute solutions of ionic constituents can be concentrated by sorption, followed by elution of the adsorbate from the resin. In fractionation, two ionic

species can be separated on the basis of charge (valence), size, acidity, exchange rate (kinetics) and exchange potential. Separation occurs during the sorption or elution cycle; chromatography is a good example of fractionation.

Template-imprinted ion-exchange resins find applications in a variety of industrial, domestic, environmental and laboratory operations. Water treatment is one of the most important applications. For protection of the environment, heavy and toxic metal cations must be removed from industrial wastewater. Generally, ion-exchange chromatography is used, and a two-step treatment with cation- and anion-exchange polymer resins is performed. The resins are usually prepared by emulsion polymerization then modified by attaching ionic functional groups.

Most cation exchange resins are prepared by sulfonation of S-DVB-based polymers. Anion-exchange resins are prepared from a chemical reaction sequence: chloromethylation, then alkylation, followed by the addition of a quaternary ammonium group.

A lot of parameters of resins are important for ion-exchange, such as chemical and thermal stability, mechanical resistance, particle size to allow the diffusion of solute, and efficiency and selectivity of the sorption process.

Molecular imprinting chromatography (MIC) has been extensively studied and several difficult separations have been performed, which have exhibited high separation factors and resolutions [23]. Molecular imprinting is highly suitable for separation, allowing the preparation of tailor-made supports with pre-determined selectivity. Using self-assembly imprinting protocols, highly efficient chirally discriminating phases may be produced. Since there are presently about 500 optically active drugs on the market, racemic resolution of drugs is a major potential application. Wulff and Sarhan used these polymers for

carbohydrase derivative separation [9,10] and then Mosbach and his team applied them in the separation of amino acid derivatives [14,15].

Antibody and receptor binding mimics prepared by template-imprinting are conceptually attractive complements to their natural counterparts. Over the last few years, several studies have demonstrated that template-imprinted polymers can serve as artificial binding mimics of natural antibodies and can be used as recognition elements in immunoassay-type analyses [16-18]. The molecular-imprinted polymers have several advantages over natural antibodies. For instance, the physical and chemical resistance of imprinted polymers leads to the possibility of sterilizing the polymers, the high durability ensures a high stability of the recognition properties, and the production cost is considerably lower.

One of the challenges in the application of template-imprinted polymers is their use as enzyme mimics. In parallel to the exciting work done with catalytic antibodies, attempts with molecular-imprinted polymers have been made to achieve catalytic activity exerted by the imprinted sites. Several strategies have been pursued in this line. The most common approach has been the use of transition state analogues (TSAs) in the imprinting protocol, thus stabilizing the reaction transition and enhancing the rate of product formation [19].

Another application developed in the area of template-imprinting is the use of molecular-imprinted polymers as recognition elements in biosensor-like devices [20-22]. Normally, a sensing element, such as an enzyme, antibody or receptor, is immobilized at the interface between the sensor and the analyte sample. A selective chemical signal, resulting from the binding process of the analyte to the recognition element is subsequently transduced into an electrical signal, amplified and converted to a "manageable" format. The

characteristics of these devices are the close proximity between the sensing part and the transducing element. The possibility of substituting natural sensing elements with template-imprinted polymers has a number of potential advantages similar to those found with the fore-mentioned antibody substitutes. Thus, they are far more stable and may perform in harsh environment, and in cases where no biological recognizing element is found, they are the only alternative. Further, a close intermarriage between sensing and transducing function can be envisaged. Given the advantages of template-imprinted polymers over their natural counterparts, imprinted polymers have the potential to become highly resistant sensing element alternatives.

1.2 Reverse Micelles as Templates

1.2.1 AOT reverse micelles

Sodium *bis*(2-ethylhexyl) sulfosuccinate (Aerosol OT or AOT), an anionic surfactant, has been widely used in research and technological applications. AOT is a amphoteric molecule, which contains two hydrophobic aliphatic chains and one hydrophilic polar head (Figure 1.2). The polar head consists of two ester groups and a sodium counter-ion (Na^+), which can be easily replaced by other alcaline ions, thereby changing the structure and the proprieties of the formed reverse micelles [24,25].

AOT is a surfactant capable of forming reverse micelles. These reverse micelles are generally nanometer-sized water droplets dispersed in an polar solvent, forming a thermodynamically stable and optically transparent solution. The formation of reverse micelles depends on the molecular geometry of the surfactant. The molecule of AOT has the shape of a truncate cone (Figure 1.2). Therefore, molecules of AOT are orientated in a

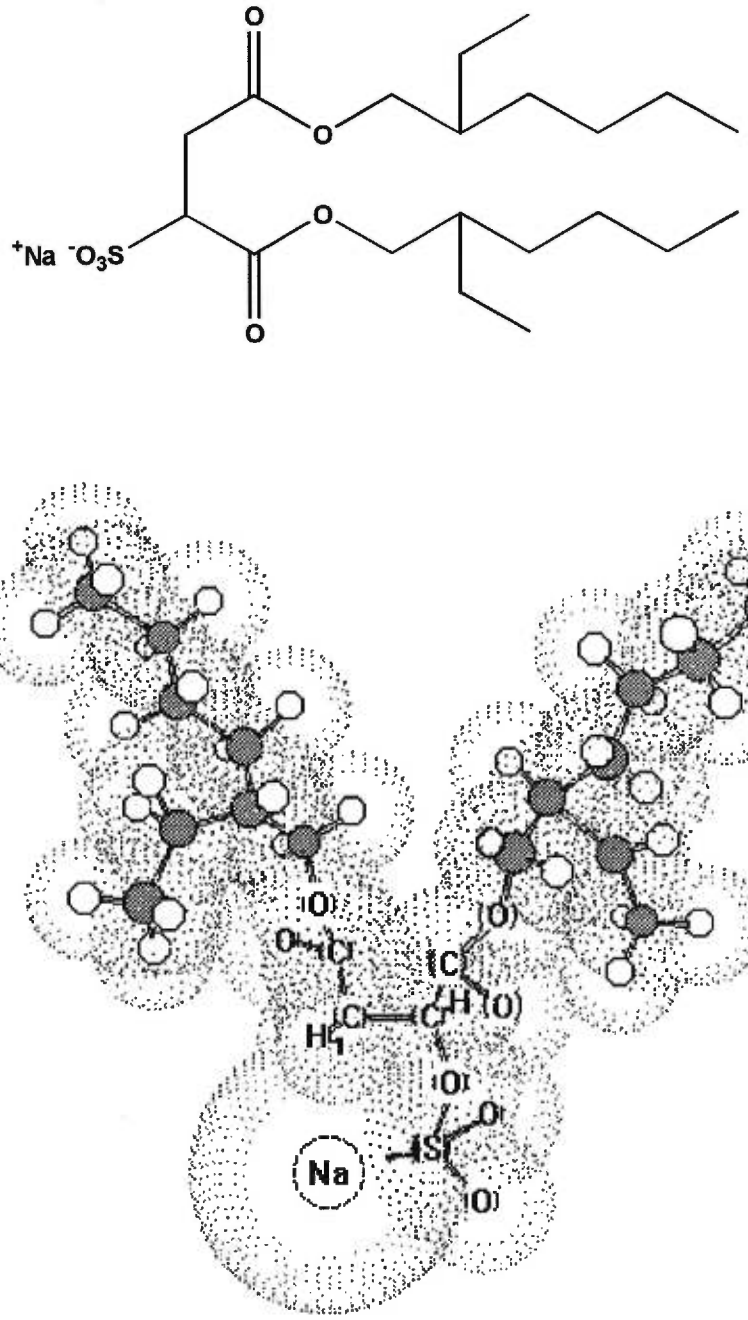

Figure 1.2 The chemical structure of sodium *bis*(2-ethylhexyl) sulfosuccinate (AOT)

mixture of organic solvent and water: the hydrophilic center is oriented to the aqueous phase, and the two hydrophobic chains are oriented to organic phase. The quantity of soluble water in reverse micelles is defined by molar concentration ratio of water to AOT (W), W = $[H_2O]/[AOT]$, in a given volume [26].

A microemulsion system contains the organic solvent, water and the surfactant at least. The size of reverse micelles in AOT/water/oil microemulsions (about 10-100 nm) [27] has been determined by various techniques such as sedimentation ultracentrifugation [28], static and dynimic light scattering [29-31], small-angle neutron scattering (SANS) [32], small-angle X-ray scattering [33], and time-resolved luminescence methods [34]. All these techniques point out that the micellar size depends primarily on the water to AOT molar ratio W. However, the nature of the oil phase, the temperature, and the ionic forces can also affect the droplet size.

According to an IR study of AOT/water/oil system by Ikushim *et al.* [35], the adsorption band of OH group was very wide and asymmetric which indicated that water in the reverse micelles was in different forms. Three types of water molecules exist in the micelles (Figure 1.3): In the core of the micelles, the water molecules are quite free as in bulk water (free water); The water molecules close to AOT molecules are bound to the sulfonic groups of the surfactant through hydrogen bonds (bound water); The water molecules trapped between the polar head groups of AOT molecules (isolated water). In the reverse micelles, at small W, added water molecules are solubilized as bound water; as W are increased, they are solubilized as isolated water as well as bound water; at much higher W, the number of free water molecules becomes comparable to that of bound water molecules, while the number of

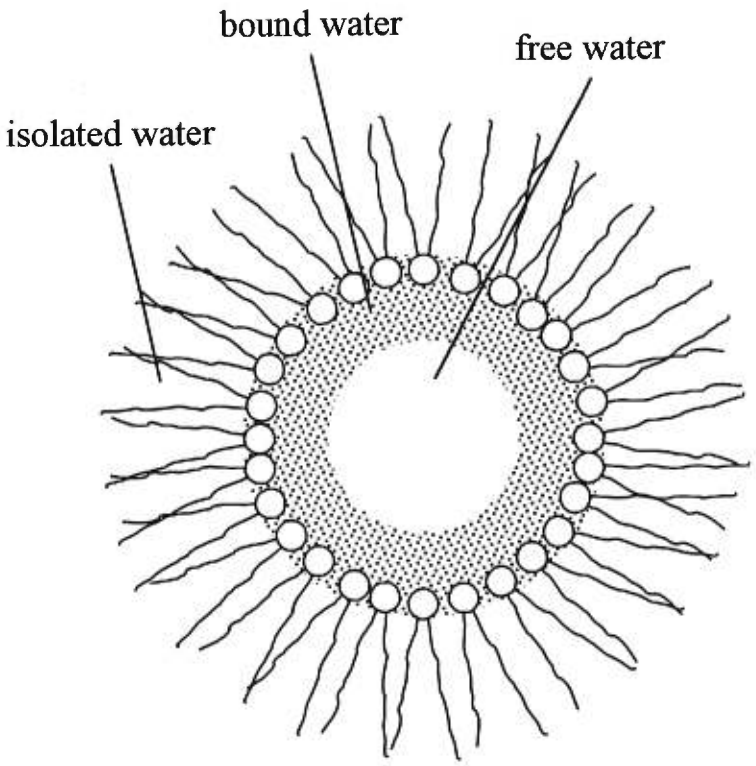

Figure 1.3 Sketches of an AOT reverse micelle in which water molecules are solubilized in three different types: free, bound and isolated water molecules.

isolated water molecules is relatively small.

The AOT reverse micelles were used as microreactors in the preparation of new materials and in biotechnologic applications [26]. Pileni *et al.* prepared nanoparticles by using different metal cations in aqueous center of reverse micelles [36,37]. The obtained crystals had potential applications in the fabrication of optical filter, antireflection coating, solar adsorbents, and microelectronic devices [38]. In addition, the AOT reverse micelles were used for the determination of enzymatic activity [39,40] and for the extraction of proteins [41,42].

1.2.2 Polymerizable surfactants

The polymerizable surfactants are amphiphilic in nature. They have both hydrophilic and hydrophobic functional groups. After polymerization, the linear homopolymers are amphiphilic, water-soluble, characterized by relatively low viscosity of their aqueous solutions. The molecular structure of amphiphilic polymers depends on the nature of hydrophilic head and hydrophobic tail. The hydrophilic functional group can be either ionic or non-ionic. The ionic polymers are characterized by their high hydrophilicity and the absence of lower critical solution temperatures. But they are subject to polyelectrolyte effects upon dilution, and tend to gelatinize upon concentration. Ionic polymers also exhibit a high sensitivity to added salt. In contrast, non-ionic polymers in water are rather insensitive to added salt and lack polyelectrolyte effect. But they generally show reduced hydrophilicity and hence exhibit lower critical solution temperatures [43].

By attaching the surfactant fragments in different ways to the backbone, various polymer geometries are realized. They include "frontal" attachment at the hydrophilic head

group (head type), "terminal" attachment at the end of the hydrophobic tail (tail-end type), intermediate structures (mid-tail type) and full incorporation into the backbone (main chain type) [44] (Figure 1.4).

The amphiphilic polymers can be prepared by polymerization of reactive surfactants, by copolymerization of hydrophilic and hydrophobic monomers, or by appropriate modification of preformed polymers, such as grafting hydrophobic chains onto hydrophilic polymers. The first method produces polymers with the best defined molecular structures. The polymerizable groups of amphiphilic monomers can be hydrophilic or hydrophobic [45]. Vinyl, allyl, styryl, acrylate, and methacrylate groups are hydrophobic. Acrylamido and methacrylamido groups are hydrophilic. The polar head groups can be non-ionic, cationic, anionic, or zwitterionic [44].

The amphiphilic polymers are widely used in emulsion polymerization as dispersing agents and emulsifiers [46,47]. In ion-exchange chromatography, some amphiphilic resins such as polymers with chelating groups, are employed for the selective formation of complexes [48,49].

The amphiphilic materials also found applications in medicine and pharmaceutics. Chen *et al.* has studied anticoagulation ability of poly(sodium 6-sulfohexyl methacrylate) and poly(sodium sulfoethyl methacrylate) [50]. The amphiphilic polymers are also used to fix or stabilize enzymes and antibodies [51], for salting out of drugs [52,53], and as antimicrobial agents [54].

1.2.3 Pore-forming reagents (porogenic agents)

The industrial ion-exchange resins can be classified as gel-type and macroporous

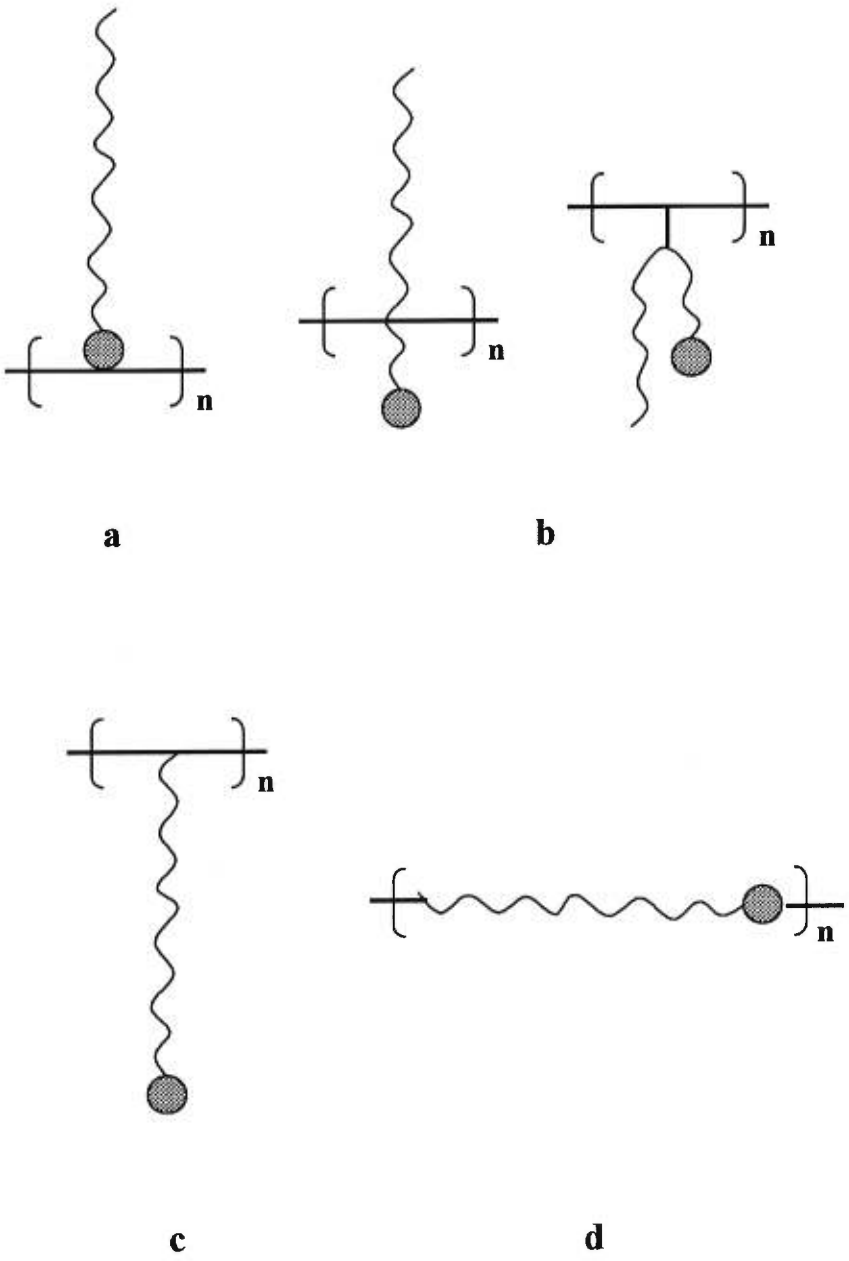

Figure 1.4 The different geometries of amphiphilic polymers: **a,** head type; **b,** mid-tail; **c,** tail-end; **d,** main chain type.

resins [78]. Most commercial ion-exchangers are based on styrene-divinylbenzene copolymers. The gel-type resins are generally lightly crosslinked (1-5% DVB) and appear transluscent. They have no permanent porosity but can swell to varying degrees in many organic solvents. They are often referred to as microporous, because the space between the crosslinks occupied by the swelling solvent are considered as small pores. Macroporous resins are obtained when the polymerization is carried out with 5-60% of DVB and in the presence of pore-forming reagents, also known as porogenic agents or diluents. During the polymerization, phase separation occurs and, after extraction of the porogenic agent and drying, permanent pores of various sizes are created. Upon swelling in an organic medium, the size of these pores may change, but their shape can be maintained. Small organic molecules can diffuse more or less freely inside.

The porogenic agents are usually chosen from a group comprising one or more of the following: thermodynamically poor solvents (precipitants), thermodynamically good solvents, and soluble polymers. The type of porogenic agents used has a critical effect on the porous properties of the resulting macroporous material. For example, polymers prepared in the presence of a precipitant have specific surface areas of up to about 100 m^2/g and their pore size distribution is characterized by a large proportion of mesopores (2-50 nm) as well as smaller macropores (>50 nm) [55-57]. In contrast, the use of good solvents as porogens gives rise to porous materials with smaller pores (mesopores and micropores smaller than 2 nm) which contribute to their high specific surface area reaching several hundreds of m^2/g [55,58]. Porous materials prepared with linear polymers as porogens are characterized by the presence of very large pores that may even reach the micrometer range. Therefore, they possess only small surface areas, typically less than 10 m^2/g. As the mechanism of the pore

formation in the presence of linear polymers is still unclear, only limited data related to polymers as porogenic agent is available [55,58].

1.2.4 Polymers made by microemulsions

The porous polymer resins can be made by emulsion polymerization and microemulsion polymerization [59]. In the last 20 years, there has been much interest in the investigation of macroporous polymer materials obtained by microemulsion polymerization, which can be used to obtain porous polymers with specific pore sizes [60]. The formation and stability of microemulsion are affected by temperature, cosurfactant, and the composition of the emulsion system.

In 1990, Menger, Tsuno and Hammond prepared crosslinked polymer resins from styrene-divinylbenzene solution of AOT reverse micelles [61]. These resins were used in the catalysis of phosphate ester hydrolysis and in chromatographic packing materials. There have also been reports on the preparation of similar crosslinked polymers possessing positively-charged and negatively-charged functional groups [6].

Chieng *et al.* studied the structure and morphology of microporous materials from microemulsion polymerization of mostly methyl methacrylate (MMA) and ethylene glycol dimethacrylate (EGDMA). Sodium 11-(N-ethylacrylamido) undecanoate (Na11-EAAU) was employed as the surfactant, 2-hydroxyethyl methacrylate (HEMA) played the role of polymerizable cosurfactant, as well as dibenzyl ketone (DBK) and sodium dodecylsulfate (SDS) which are nonpolymerizable. According to their reports, the microstructure of the microporous materials can be controlled by the molar ratio of Na11-EAAU to SDS [55].

1.3 Gas Adsorption

Different methods can be used to determine the surface area and the pore size of a porous solid. The most widely used method is low-temperature gas sorption, particularly nitrogen and krypton, at liquid-nitrogen temperature. When a porous solid is exposed to a gas, the gas molecules impinge into the porous solid body and may reside upon the surface for a finite time. This phenomenon is called adsorption. The quantity of gas taken up by a sample of solid is proportional to the mass of the sample, and it depends also on the temperature, the vapor pressure, and the nature of both the solid and the gas. The adsorption isotherm is the relationship, at constant temperature, between the amount of gas adsorbed and the pressure, or relative pressure, respectively. Generally, gas adsorption can measure the total surface area and pore sizes within the diameter range from 0.4 to 200 nm, and very high-resolution result can be obtained.

1.3.1 Adsorption forces

Adsorption processes may be either physical or chemical, depending on the nature of the forces involved. The forces involved in the physical adsorption may be of the non-specific type (van der Waals), which includes attractive forces (or dispersion forces) and electrostatic ones. The dispersion forces are due to the rapid fluctuation in electron density within each atom, which induces an electrical moment in a near neighbor and thus leads to attraction between the atoms. The electrostatic forces are present in a polar solid consisting of ions, or containing polar groups or π-electrons. It will give rise to an electric field which will induce a dipole in the gas molecule. The van der Waals interactions are weak. The

formation of a physically adsorbed layer may be compared to the condensation of a vapor to form a liquid [62].

On the other hand, chemical adsorption involves specific chemical interactions between the adsorbate and the adsorbent and, correspondingly, the energies of adsorption may be quite large and comparable to those of chemical bond formation.

When adsorption takes place, the gas molecules are restricted to two-dimensional motion. Gas adsorption processes are, therefore, accompanied by a decrease in entropy (ΔS_{ads}). Since adsorption also involves a decrease in free energy (ΔG_{ads}), from the thermodynamic relationship, one has

$$\Delta G_{ads} = \Delta H_{ads} - T\Delta S_{ads} \tag{1.1}$$

Therefore, ΔH_{ads} must be negative, i.e., the adsorption of gases and vapors on solids is always an exothermic process. The enthalpy of adsorption can be measured by direct calorimetric method or from reversible adsorption isotherms using the Clausius-Clapeyron equation:

$$\left(\frac{\partial \ln P}{\partial T}\right) = -\frac{\Delta H_{ads}}{RT^2} \tag{1.2}$$

The free energy of physical adsorption of a gas is usually similar to its heat of condensation (about 20 kJ mol^{-1}). The enthalpy of chemical adsorption is, in general, much larger (about 200 kJ mol^{-1}) [63].

1.3.2 External and internal surfaces

The external surface is defined as blankets around particles or agglomerates of solids. But, since the surface of a porous solid is rough and irregular, this definition is not very clear

at all. It was suggested that the external surface should include all the prominences and all cracks which are wider than they are deep. The internal surface comprises the walls of all cracks, pores and cavities which are deeper than they are wide [60]. The surface area depends on the method of calculation and the shape of the pore size distribution curve. The size and shape of gas molecules also affects the accessibility of pores, and thus the measured surface area.

1.3.3 Classification of pore sizes

The pores can be classified into three groups according to their sizes, i.e., the average diameter of a cylindrical pore: (a) macropores having widths in excess of 50 nm; capillary condensation does not take place in these pores which are essentially avenues of transport to smaller pores; (b) mesopores, also known as transition or intermediate pores having widths between 2 and 50 nm; these mark the limit of applicability of the Kelvin equation; (c) micropores, less 2 nm. Since the concept of the surface of a solid body is a macroscopic notion, surface area loses its significance when micropores are present. However, pore volume is still an applicable concept [64].

The adsorption in different types of pores can be identified in the isotherm. For micropores, as a result of the closeness of cavity walls, the solid-gas interaction is more important than in the others. The quantity of adsorbed gas increases rapidly at low relative pressure [65]. And for mesopores, the isotherm presents a hysteresis loop because the adsorbate is condensed on the walls of the pores (capillary condensation). For macropores, because the pores are wide, the relative pressure is so close to unity, that the isotherm is difficult to be recorded accurately [62].

1.3.4 Adsorption isotherms

Three phenomena may be involved in physical adsorption: the monomolecular adsorption, the multimolecular adsorption and the condensation in pores or capillaries. The majority of the corresponding adsorption isotherms may be grouped in the six types shown in Figure 1.5. The first five types were given by Brunauer et al. [66] and type 6 was identified later [64].

Type 1 isotherm is characterized by a rapid initial rise in the amount of gas adsorbed at low pressure followed by a flat region. It is generally accepted that the shape is characteristic of micropore filling and the limiting amount adsorbed is a measure of micropore volume. Type 1 isotherms may also occur for adsorption on high energy level surfaces.

The reversible type 2 isotherm is obtained by adsorption on many nonporous or mesoporous powders and represents unrestricted multilayer adsorption on a heterogeneous substrate. Although layers at different levels may exist simultaneously, monolayer completion occurs at the point of inflection of the isotherm. This is known as point B and was first identified by Emmett and Brunauer [79]. They subsequently developed a theory, containing a constant c, to locate this point. Type 2 isotherms occur for high c values and the 'knee' at the point of inflection becomes more pronounced as the c value increases. Increasing c values indicate increasing adsorbate-adsorbent affinity [62].

Type 3 isotherms arises when adsorbate-adsorbent interaction is weak and c is less than 2.

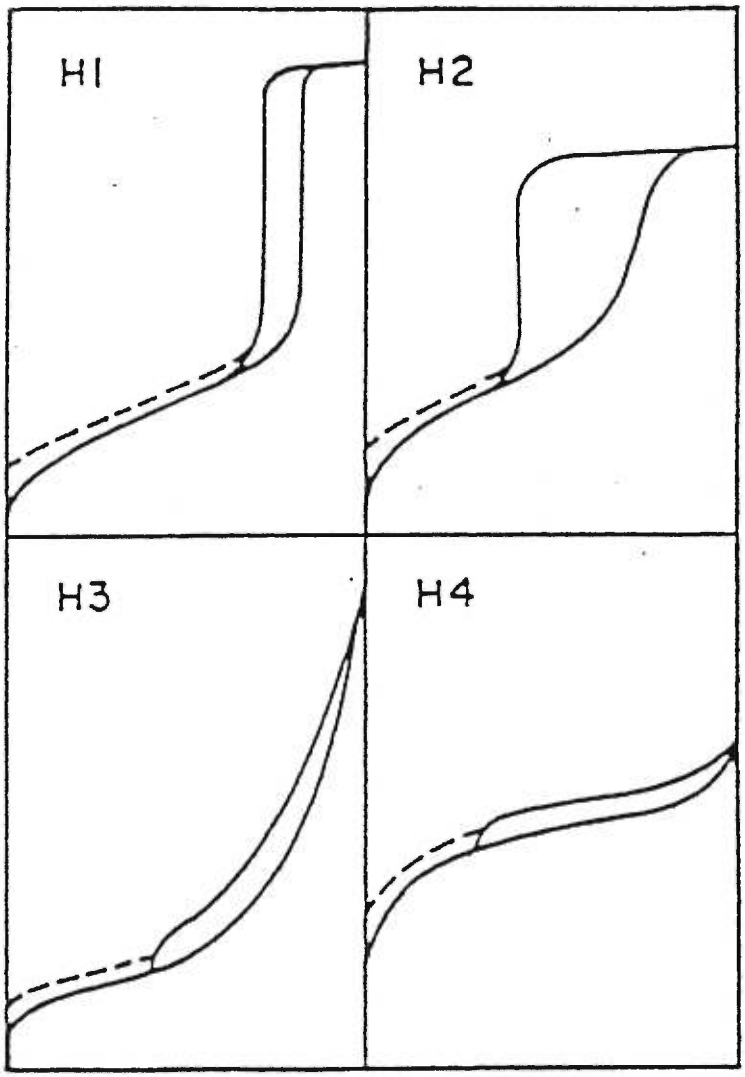

Figure 1.5 Different types of adsorption isotherms. Point B indicates the completion of the monolayer, so that the adsorption at point B should be equal to the monolayer capacity [64].

A characteristic feature of type 4 isotherms is the hysteresis loop. This has been explained as being due to capillary phenomena and this part of the isotherm is used for the evaluation of pore size distribution. As the pressure is reduced from the saturation value, the gas molecules condensed in the capillary cracks of the adsorbent do not evaporate as readily as they would from the bulk liquid due to the lowering of the vapor pressure over the concave meniscus formed by the condensed liquid in the pores.

Type 5 isotherms are similar to type 4 except that the adsorbate-adsorbent interaction is weak.

Type 6 isotherms arise with stepwise multilayer adsorption of noble gas molecules on a uniform substrate.

1.3.5 Hysteresis loops and capillary condensation

For many adsorbents, a hysteresis loop occurs between the adsorption and desorption branches of the isotherm [63]. This is due to capillary multilayer adsorption as a result of condensation augmenting at the pressures where the hysteresis is present.

The vapor pressure over a convex liquid surface is greater than that over the corresponding flat surface. The relation between the two vapor pressures is given by Laplace equation:

$$P_{vap} = P_{liq} \times \frac{2\gamma}{r} \tag{1.3}$$

where P_{liq} is the pressure of pure liquid, P_{vap} is the pressure of vapor, γ is the tension of liquid surface and r is the radius of the liquid curvature.

A liquid which wets the wall of a capillary will have a concave liquid-vapor interface (meniscus). And this indicates that the pressure on the meniscus is lower than the

atmospheric pressure $2\gamma/r$ times, r being the radius of capillary. The Kelvin equation is derived from the Laplace equation. It gives the relation between the meniscus concave radius and the relative pressure[62]:

$$RT\ln\left(\frac{P}{P_0}\right) = -\frac{2\gamma\ V_L\cos\theta}{r} \tag{1.4}$$

where P/P_0 is the relative pressure, θ is the contact angle between the liquid and the capillary wall, and V_L is the adsorbate molar volume. Condensation can take place in narrow capillaries at pressures which are lower than the normal saturation vapor pressure. Zsigmondy suggested that this phenomenon might also apply to porous solids [80].

The first possible explanation of hysteresis loop phenomenon is given in terms of contact angle hysteresis. The contact angle upon adsorption, when liquid is advancing over a dry surface, is usually greater than the contact angle during desorption, when liquid is receding from a wet surface. From the Kelvin equation, it is evident that the pressure below which a liquid vaporizes from a particular capillary will, under these circumstances, be lower than the pressure required for capillary condensation [62].

Another theory of adsorption hysteresis considers that there are two types of pores present, each having a size distribution [62]. The first type is V-shaped pores, which fill and empty reversibly. The second type has a narrow neck and a relatively wide interior. These 'ink-bottle' pores are supposed to fill completely at a P/P_0 value corresponding to the relatively wide pore interior, but once filled they retain their contents until P/P_0 is reduced to a value corresponding to the relatively small width of the pore neck.

In a third theory, the pores are considered to be open-ended cylinders. Condensation will commence on the pore walls, for which the principal radius of curvature are the pore

radius and infinity, and continue until the pore is filled with condensed liquid. Evaporation must take place from the concave liquid surfaces at the ends of the pore, for which (assuming zero contact angle) the principal radii of curvature are both equal to the pore radius.

The hysteresis loops found in the literature are of various shapes [68]. The classification originally proposed by de Boer in 1958 has proved useful. A new classification of hysteresis loop, as recommended in the IUPAC manual, consists of the four types shown in the Figure 1.6 [64]. To avoid confusion with the original de Boer classification, the characteristic types are now designated H1, H2, H3 and H4.

Certain shapes of hysteresis loops are associated with specific pore structures. Thus, type H1 loops are often obtained with agglomerates or compacts of spheroidal particles of fairly uniform size and array. Some corpuscular systems tend to give H2 loops, but in these cases the distribution of pore size and shape is not well defined. Types H3 and H4 have been obtained with adsorbents having slit-shaped pores or plate-like particles (in the case of H3). The Type I isotherm character associated with H4 is indicative of microporosity.

1.4 Physical Models of Gas Adsorption

1.4.1 The Langmuir model

The first theoretical equation relating the quantity of adsorbed gas to the equilibrium pressure of the gas was proposed by Langmuir. In his model, the adsorption is limited to a monolayer and this equation has limited applicability to physical adsorption but has wider

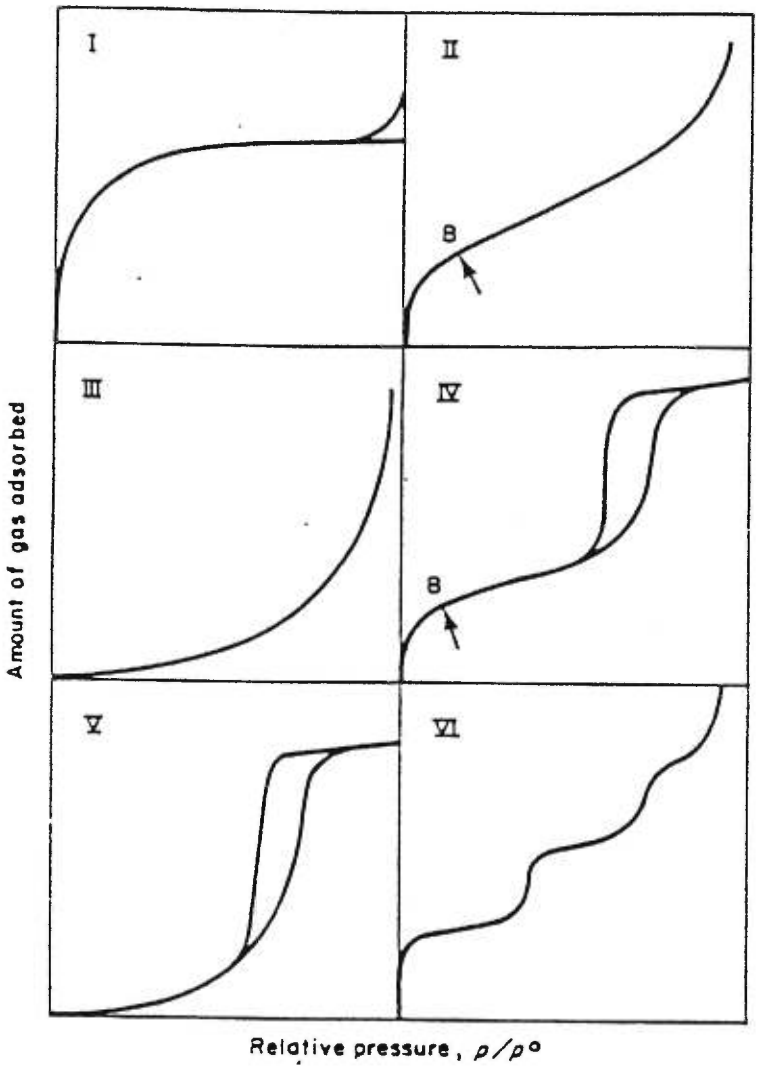

Figure 1.6 The classification of different type of hysteresis loops as recommended by IUPAC [64].

applications in chemical adsorption and the adsorption of solute, including dye molecules, from solution.

In this method it is assumed that the number of molecules evaporating from the surface is equal to the number condensing on the surface. The Langmuir adsorption isotherm is based on the characteristic assumptions that (a) only monomolecular adsorption takes place, (b) adsorption is localized and (c) the heat of adsorption is independent of surface coverage. A kinetic derivation in which the velocities of adsorption and desorption are equated with each other determines the Langmuir equation [69,70]:

$$\frac{P}{V} = \frac{P}{V_m} + \frac{1}{aV_m} \tag{1.5}$$

where P is the pressure, V the equilibrium volume of gas adsorbed per unit mass of adsorbent, V_m the volume of gas required to cover a unit mass of adsorbent with a complete monolayer, and a is a constant dependent on the temperature but independent of surface coverage:

$$\frac{1}{a} = k \exp\left(\frac{\Delta H_{abs}}{RT}\right) \tag{1.6}$$

where k is a constant of proportionality. The Langmuir equation can be also written as

$$\frac{V}{V_m} = \frac{aP}{1+aP}. \tag{1.7}$$

From Langmuir equation 1.5, a plot of P/V against P yields the monolayer capacity V_m.

At low pressure, the Langmuir equation is written as $V = aV_mP$, which indicates that the volume of gas adsorbed varies linearly with pressure. At high pressures a limiting monolayer coverage, $V = V_m$, is reached. The curvature of the isotherm at intermediate pressures depends on the value of the constant a and on the temperature.

1.4.2 The BET model [62,71]

The most important step in the study of adsorption came with the model of Brunauer, Emmett and Teller, for the multilayer adsorption of gases on solid surfaces. This multilayer adsorption theory known generally as the BET theory has occupied a central position in gas adsorption studies and surface area measurements ever since it was formulated.

The BET equation is derived by balancing the rates of evaporation and condensation for the various adsorbed molecular layers, and is based on the simplified assumption that a characteristic heat of adsorption ΔH_l applies to the first monolayer, while the heat of liquefaction, ΔH_L, of the vapor applies to adsorption in the second and subsequent molecular layers. The equation is usually written in the following form

$$\frac{P}{V(P_0 - P)} = \frac{1}{V_m c} + \frac{(c-1)}{V_m c}\frac{P}{P_0} \tag{1.8}$$

where P is the vapor pressure, P_0 the saturation vapor pressure, V_m the monolayer capacity and $c \approx \exp[(\Delta H_L - \Delta H_l)/RT]$. A plot of $P/[V(P_0-P)]$ against P/P_0 should yield a straight line having a slope of $(c\text{-}1)/(V_m c)$ and an intercept of $1/(V_m c)$.

To relate this to surface area it is necessary to know the area σ occupied by one molecule. Surface area from the monolayer capacity can be calculated by

$$S_{BET} = \frac{N\sigma V_m}{M_V} \tag{1.9}$$

where S_{BET} is specific surface area in m^2/g, N the Avagadro's number, σ the area occupied by one adsorbate molecule (usually taken as 1.62×10^{-19} m^2 for nitrogen), V_m the monolayer capacity in cm^3 per gram of solid, M_V the molar volume (22410 cm^3/mol for nitrogen).

1.4.3 The BJH model [62, 72]

The possibility of calculating the pore size distribution of a porous solid from the capillary condensation region of its Type 4 isotherm has long been recognized. Barrett, Joyner and Halenda developed a method, the BJH method involving the length and area of pore walls. This method considers a relation between adsorbed layer thickness and relative pressure, and the Kelvin equation which connects vapor pressure and capillary radius:

$$RT \ln\left(\frac{P}{P_0}\right) = - \frac{2\gamma V_L}{r_c} \tag{1.10}$$

where r_c is the core radius, γ the surface tension and V_L the adsorbate molar volume. As the liquid nitrogen adsorption occurs at 77 K, γ is equal to 8.88 mN m^{-1} and V_L to 34.68 mL mol^{-1}. Therefore, Kelvin equation is rewritten as:

$$\ln(P/P_0) = -0.961/r_c(nm) \tag{1.11}$$

where the unit of r_c is in nm. And the cylindrical pore radius is defined as

$$r_P = r_c + t \tag{1.12}$$

where t is the adsorbate thickness (Figure 1.7).

The BJH model is based on the following hypotheses: (a) the pores have a cylindrical shape and (b) the adsorbate is restricted in the pores by monolayer and multilayer physical adsorption and by capillary condensation.

As the pressure falls from P_0 to P_1, a condensed volume, V_c, is desorbed, and V_{c1} is the core volume of pores with radii greater the r_{p1} and of average size $\bar{r}_{p1}$ (Figure 1.7).

Hence,

$$V_{c_1} = \pi \bar{r}_{c_1}^{\,2} L_1(r) \tag{1.13}$$

$$S_{P_1} = 2\pi\ \bar{r}_{P_1} L_1(r) \tag{1.14}$$

$$V_{P_1} = \pi\ \bar{r}_{P_1}^{\,2} L_1(r) \tag{1.15}$$

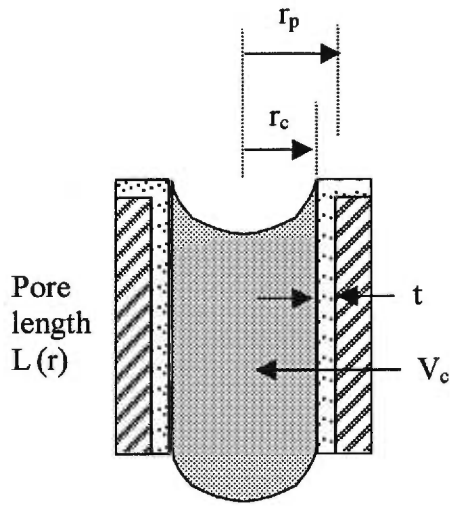

Figure 1.7 The cylindrical pore model. r_p pore radii, r_c core radii, t is the adsorbate layer thickness V_c core volume, L pore length..

And the volume of the first class of pores with average size $\bar{r}_{p1}$ is given by

$$V_{p_1} = \left(\frac{\bar{r}_{p_1}^{\,2}}{\bar{r}_{c_1}^{\,2}} \right) V_{c_1} \tag{1.16}$$

The surface of the first class of pores is given by

$$S_{P_1} = \frac{2V_{P_1}}{\bar{r}_{P_1}} \tag{1.17}$$

$\bar{r}_{c1}$ is given by the Kelvin equation

$$\bar{r}_{c_1} = -\frac{\gamma V_L \cos\theta}{RT} \left(\frac{1}{\ln x_0} + \frac{1}{\ln x_1} \right) \tag{1.18}$$

where x_1 equals P_1/P_0, x_0 is approximately equal to unity, and:

$$\bar{r}_{P_1} = \bar{r}_{c_1} + \bar{t}_1 \tag{1.19}$$

t_1 is the adsorbate layer thickness, obtained from an appropriate *t*-curve. As the pressure falls from P_1 to P_2, a condensed volume, V_{c2}, is desorbed. This consists of two parts: (1) The core volume of the pores in the size range of r_{P1} to r_{P2} having a mean size of $\bar{r}_{P2}$, i.e., the Kelvin volume V_K; and (2) an amount $S_{p1}\Delta t_2$ desorbed from the exposed surface of the second class of pores ($\Delta t_2 = t_2 - t_1$).

Hence,

$$V_{c_2} = \pi\ \bar{r}_{c_2}{}^2 L_2(r) + S_{P_1}\Delta t_2 \tag{1.20}$$

$$V_{P_2} = \pi\ \bar{r}_{P_2}{}^2 L_2(r) \tag{1.21}$$

$$S_{P_2} = 2\pi\ \bar{r}_{P_2} L_2(r) \tag{1.22}$$

Therefore,

$$V_{p_2} = \left(\frac{\bar{r}_{p_2}}{\bar{r}_{c_2}}\right)^2 \left[\, V_{c_2} - S_{P_1}\Delta t_2 \right] \tag{1.23}$$

where

$$V_{K_2} = V_{c_2} - S_{P_1}\Delta t_2 \tag{1.24}$$

and

$$S_{P_2} = \frac{2}{\bar{r}_{P_2}} V_{p_2} \tag{1.25}$$

For the whole desorption process, or the *n*th desorption step

$$V_{p_n} = \left(\frac{\bar{r}_{p_n}}{\bar{r}_{c_n}}\right)^2 \left[V_{c_n} - \Delta t_n \sum_{x=0}^{n-1} S_{P_x} \right] \tag{1.26}$$

$$S_{P_n} = \frac{2}{\bar{r}_{P_n}} V_{p_n} \tag{1.27}$$

The pore size distribution curve is a Gaussian function between volume increment ($\Delta V/\Delta D$ in mL $nm^{-1}g^{-1}$) and pore diameter (D in nm). The peak maximum gives the average diameter defined as $[\Sigma V_i D_i / \Sigma V_i]$, where V_i and D_i are respectively the volume and the diameter of each pore.

The position and form of the distribution curve depend on which hysteresis loop branch (adsorption or desorption) is used for calculation. But there is no general recommendation for such a selection. Both adsorption and desorption isotherms can be used in the analysis for comparison.

1.5 Objectives of this project

Molecular imprinting techniques have been used to make polymer resins with size and shape specificity for various applications. The porous polymer resins with specific pore sizes have already been prepared in our laboratory by the use of AOT reverse micelles as imprinting templates [25, 73-75]. These polymers are prepared by bulk polymerization in a mixture of styrene and divinylbenzene in which AOT reverse micelles are solubilized. It has been shown that the cavity size and surface area can be controlled within a certain range by varying the AOT molar concentration and water content. The pore area has its maximum value when the AOT molar concentration is 0.2 M, and it also increases linearly with the water content until W reaches 12 [25,73].

The effect of the degree of crosslinking has also been investigated. In general, the surface area and pore volume of the polymer resins were found to increase as a function of the degree of crosslinking. The influence of cosurfactants on functionalized porous polymer porosity has also been addressed. Polymerizable and non-polymerizable cosurfactants such

as *n*-butanol and 2-hydroxyethyl methacrylate were used. The addition of various amounts of cosurfactant in the concentration range of 0 to 0.06 M did not influence significantly the porosity of the polymers [74,75].

The surface area and pore volume were found to depend on the particle size of the resins but the pore size did not show such dependence. Thermal analyses of the polymer resins showed that the polymers were stable up to their decomposition temperature well, above 300 °C, and the porosity of the resin remained stable after heating for 48 hour at 120 °C [74,75].

The objective of the current project is to prepare and optimize the various polymer resins for the selective binding of metal cations. Several series of crosslinked polymer resins have been prepared by using AOT reverse micelles. Some polymerizable cosurfactants with negatively charged polar groups were synthesized and employed in the preparation of the functionalized porous polymers to test their use in the selective binding and removal of metal cations. These resins have the following characteristics: (1) Size-selectivity: The size of the functional cavities can be adjusted during the preparation of the resins; (2) Functionality: The functional groups (cationic, anionic or chelating) can be selectively introduced or modified; (3) Stability: The high degree of crosslinking ensures the polymer resins to be very stable under pressure and upon heating.

It is known that methyl methacrylate (MMA) and ethylene glycol dimethacrylate (EGDMA) can be readily polymerized to form a crosslinked copolymer. These monomers were tested to form the polymer matrix. The water content (W) was varied to control the pore sizes, but the concentration of AOT was fixed at 0.2 M.

Polymer resins with a good solvent (toluene) as porogenic agent were also prepared. The purpose of using porogenic agents is to improve the accessibility of the isolated pores formed by AOT reverse micelles. The amount of toluene was varied from 0 to 60% of the total volume.

The pore-forming reagents are nonpolymerizable, and can be easily removed after polymerization. Thus, permanent pores are created. In our case, this will leave the polymer resin with large channels giving access to the well-defined smaller pores formed by the micellar templates. Then a better accessibility of the cavities with functional groups can be achieved, and it will also improve the binding efficiency and capacity of the resins.

All the polymer resins so obtained are characterized by infrared (IR) and nuclear magnetic resonance (NMR) spectroscopy and BET gas adsorption experiments. The conditions for the selective binding of metal cations using functionalized porous polymers, such as the pH, concentration of eluent and binding time, have also been studied.

The new resins should find industrial applications in selective adsorption, removal, recovery, separation, purification and analysis. Because of their size and functional-group specificity, the new polymer resins may be eventually used in industrial sectors involved in metals fabrication/finishing and mining. Such materials can also be used to prepare chromatographic column for analytical purposes.

2. Experimental

2.1 Synthesis of Polymerizable Cosurfactants

2.1.1 Synthesis of 6-(*p*-vinylbenzyloxy)hexanol

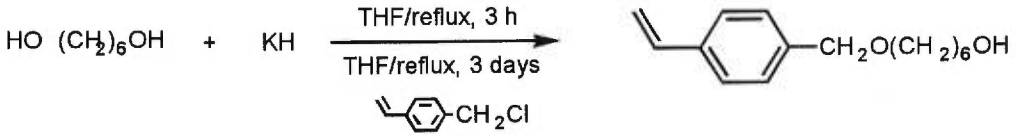

Potassium hydride (11.46 g, 0.10 mol) dispersion in mineral oil (35 wt %) was slowly added into a solution of 1,6-hexanediol (17.91 g, 0.15 mol) in 250 mL THF at room temperature. The mixture was stirred and refluxed during 3 hours for the formation of potassium alkoxide. Then a solution of vinylbenzyl chloride (12.59 g, 0.08 mol) and 18-crown-6 (~1 g) in 100 mL THF was added dropwise to the mixture with an addition funnel during 1 hour. This mixture was stirred and refluxed for 3 days. The reaction was monitored with thin layer chromatography (TLC). THF was then evaporated and the residue was dissolved in 200 mL dichloromethane. The mixture was washed with distilled water (3×150 mL). The organic phase was collected, dried with sodium sulfate (Na_2SO_4), filtered and the solvent was evaporated. Finally the product was purified on a silica gel (Merck 60, 230-400 mesh ASTM) column with a mixture of petroleum ether and ethyl acetate (4:1) as eluent. The pure product was a clear yellow liquid. The yield was 62 % (14.53 g, 0.062 mol).

^{1}H NMR ($CDCl_3$): δ 7.4 (m, 4H), 6.7 (m, 1H), 5.8 (dd, 1H), 5.2 (dd, 1H), 4.5 (d, 2H), 3.6 (t, 2H), 3.5 (q, 2H), 2.3 (s 1H), 1.5 (m, 4H), 1.4 (m, 4H).

2.2.2 Synthesis of 6-hydroxyhexyl methacrylate

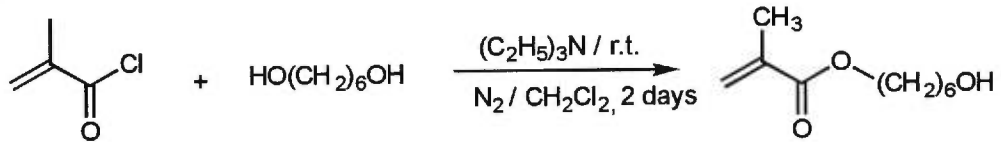

Methacrylic chloride (5.81 g, 0.05 mol) in 50 mL dichloromethane (DCM) was slowly added dropwise with an addition funnel into 200 mL DCM solution of 1,6-hexanediol (59.69 g, 0.50 mol) and triethylamine (12.27 g, 0.10 mol) at room temperature. The mixture was stirred for 2 days. The reaction was monitored by TLC. The excess of 1,6-hexanediol was then filtered, DCM was evaporated and the residue was dissolved in 200 mL of ethyl acetate. The mixture was washed with distilled water (3×150 mL) and sodium chloride aqueous solution (100 mL). The organic phase was collected and dried with anhydrous sodium sulfate, then filtered and the solvent was evaporated. The product was purified with chromatography on a silica gel packed column (Merck 60, 230-400 mesh ASTM), the eluant was a mixture of petroleum ether and ethyl acetate (4:1). The purified product was a clear colorless liquid, and the yield was 93 % (9.85 g, 0.047 mol).

^{1}H NMR ($CDCl_3$): δ 6.1 (d, 1H), 5.5 (d, 1H), 4.1 (t, 2H), 3.6 (q, 2H), 2.0 (s, 1H), 1.9 (dd, 3H), 1.5 (m, 4H), 1.6(m, 4H)

2.2 Preparation of Polymer Resins

2.2.1 Functional polymers made by using polymerizable surfactants

Styrene (S) and divinylbenzene (DVB) (both from Aldrich) were washed with a 10% NaOH aqueous solution and vacuum distilled to remove any added inhibitors. DVB was 55%

pure, and the distillation did not change its apparent composition. Sodium bis(2-ethylhexyl) sulfosuccinate (AOT) was purchased from Sigma and used as received. The free radical initiator, 2,2'-azoisobutyronitrile (AIBN), purchased from Eastman Kodak, was recrystallized from methanol and stored in dark bottles in a refrigerator.

The preparation of the polymer resins is shown schematically in Figure 2.1. A solution of styrene and divinylbenzene (1:1, v/v) containing the initiator AIBN ([AIBN = 0.05 M) was prepared. Then, AOT (2.22 g, 0.01 mol, [AOT] = 0.2 M) was dissolved in a minimal amount of this solution. When AOT was completely dissolved, the mixture was transferred to a 25 mL volumetric flask. A certain amount of the cosurfactant was added into the solution to obtain a concentration of 0.2 M. This solution was sonicated in an ultrasonic bath for several minutes until the surfactants were completely dissolved. Deionized water was then added to obtain a water-to-AOT molar ratio (W) of 12. The mixture was sonicated until it becomes a clear and transparent solution. The final volume of the solution in the volumetric flask (25 mL) was adjusted by adding the monomer solution (S-DVB).

The solution was then transferred to an ampoule and frozen in liquid nitrogen. The ampoule was then sealed and the solution was thawed to room temperature. The glass container was then placed in a UV crosslinker (UVC-515 UV Multilinker, Ultra-Lum, Carson, CA). The polymerization started immediately by UV irradiation at a wavelength of 254 nm. After 4-6 hours when the solution became opaque and looked like a gel, the test-tube was transferred into an oven, and heated at 65-70 °C overnight.

Three polymerizable cosurfactants were used individually in the preparation of these samples (Table 2.1).

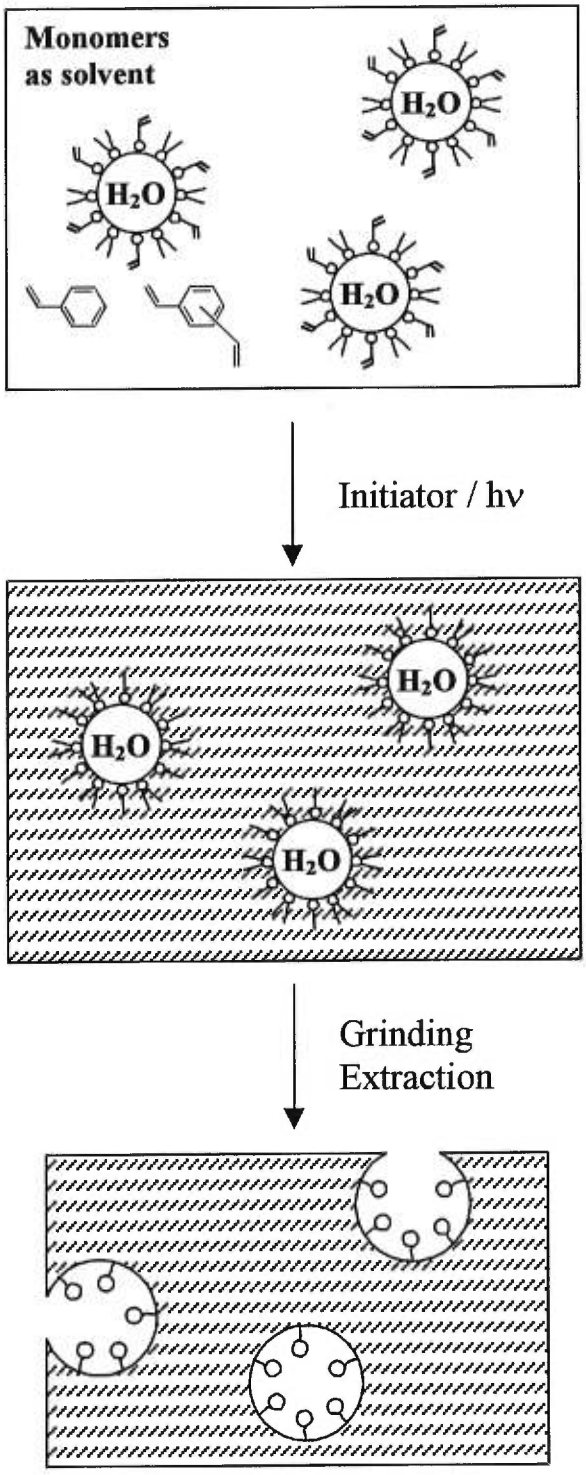

Figure2.1 The preparation scheme of functional polymers with polymerizable cosurfactants with based on S-DVB matrix.

Table 2.1 Samples prepared by using polymerizable cosurfactants with PS matrix. S-DVB (1/1, v/v), [AOT] = 0.2 M, [AIBN] = 0.05 M, W = 12.

Sample	Polymerizable Cosurfactant	Concentration of the cosurfactant (M)
C1	6-(*p*-vinylbenzyloxy)hexanol	0.20
C2	6- hydroxyhexyl methacrylate	0.20
C3	Sodium styrenesulfonate	0.07

These polymer resins were ground into powder with the aid of a Technilab micromill (Bel-Art, Pequanock, NJ) and then washed with toluene and ethanol successively in a Soxhlet extractor to remove any unreacted monomers and AOT. The ground resins were dried under vacuum and sieved into different sizes.

2.2.2 Polymer resins with PMMA matrix

Methyl methacrylate (MMA) and ethylene glycol dimethacrylate (EGDMA) (Aldrich) were washed with a 10% NaOH aqueous solution and vacuum distilled. The volume ratio of MMA to EGDMA was 4:1.

The preparation procedure of polymer resins based on PMMA was the same as the one used for S-DVB resins (Section 2.2.1) but without any cosurfactant. The concentration of AOT was fixed to 0.2 M, and distilled water was added to the system to adjust the water-to-AOT ratio (W) from 0 to 14, beyond which the solution was no longer homogeneous (Table 2.2).

Table 2.2 Polymer resins prepared with PMMA matrix. [AOT] = 0.2 M, MMA:EGDMA = 4:1 (v/v) and [AIBN] = 0.05 M, total volume = 25 mL.

Samples	W [H_2O]/[AOT]	Amount of H_2O (mol)	Weight of H_2O (g)
A1	0	0	0
A2	2	0.01	0.18
A3	4	0.02	0.36
A4	6	0.03	0.54
A5	8	0.04	0.72
A6	10	0.05	0.90
A7	12	0.06	1.08
A8	14	0.07	1.26

2.2.3 Polymer resins prepared with a pore-forming reagent

The preparation scheme of these samples is shown in Figure 2.2. Styrene (S) and divinylbenzene (DVB) were used as the matrix for these samples, and the ratio of monomers (S:DVB) was 1/1 (v/v). Toluene was added as the pore-forming reagent, varying from 0 to 60 vol. % of the total volume (Table 2.3). The preparation of polymer resins was described previously but without cosurfactant. The concentration of AOT was 0.2 M, W = 12 and [AIBN] = 0.05 M.

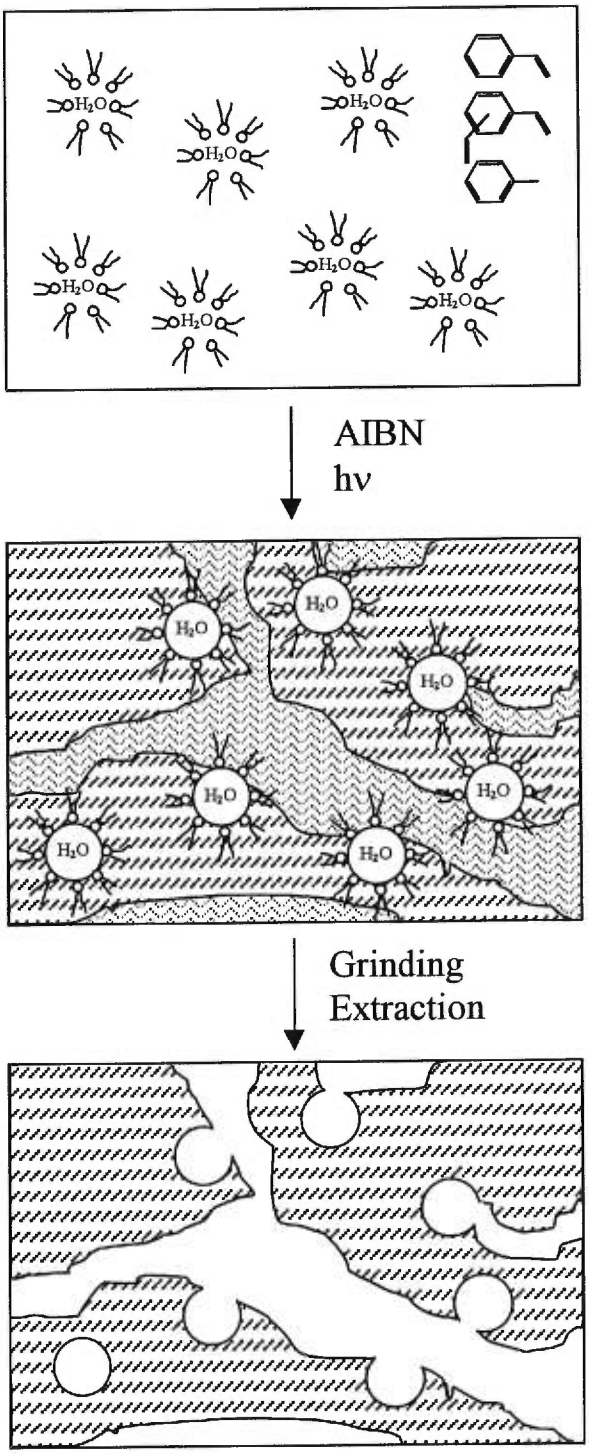

Figure 2.2 The preparation scheme of polymer resins with pore-forming reagent (toluene).

Table 2.3 Samples prepared with toluene (T) as pore-forming reagent. S:DVB = 1/1 (v/v), [AOT] = 0.2 M and [AIBN] = 0.05 M, total volume = 25 mL.

Samples	Volume of toluene added (mL)	[Toluene] (vol. %)
T1	0	0
T2	1.25	5
T3	2.50	10
T4	5.00	20
T5	7.50	30
T6	10.00	40
T7	12.50	50
T8	15.00	60

2.3 Characterization of the polymers

All polymer resins were characterized by solid state ^{13}C NMR, IR spectroscopy and BET gas absorption/desorption experiments. The polymerizable cosurfactants prepared for this study were characterized by ^{1}H NMR in solution.

2.3.1 Nuclear magnetic resonance (NMR) spectroscopy

The ^{1}H NMR spectra of cosurfactants were recorded on Varian VXR-300, Bruker AMX-300 and Bruker AMX-400 spectrometers. The solvents used were deuterated-chloroform ($CDCl_3$) and deuterated water (D_2O).

Solid state NMR spectra were recorded at room temperature on a Varian VXR-300 spectrometer equipped with a Doty CP/MAS probe operating at 75 MHz for ^{13}C and a spinning rate of ca. 4 kHz. The contact time (1.5 ms), relaxation delay (5 s), and other parameters were optimized for the comparison of the ^{13}C NMR spectra.

2.3.2 Infrared spectroscopy

The infrared spectra were recorded on a Bomen Fourier transform IR spectrometer (model MB-100, from Hartmann & Braun). KBr pellets were prepared with the powder (mesh size 60-100, 150-250 μm) of the resins, and 30 scans were accumulated at room temperature.

2.3.3 BET gas absorption

The BET gas absorption measurements were performed on a Coulter SA-3100 surface area and pore size analyzer (Coulter Scientific, Miami, FL) with nitrogen to determine the surface area, pore volume, pore size and pore size distribution of the polymer resins. The absorption and desorption experiments were done at liquid nitrogen temperature (77 K). Polymer resins with mesh size between 60 and 100 (150-250 μm) were normally used for the measurements. First the polymer resins were outgased at 50 °C for 15 min. Helium was used to determine the free space in the sample cell. Then, the absorption and desorption isotherms were constructed by measuring the quantity of gas condensed as a function of relative pressure. The precision of the result from BET experiment depend on the BET equation, and for the surface area is 0.1 m^2/g, for pore volume is 0.001 mL/g, for average diameter is 0.1 nm.

2.4 Ion exchange experiments

2.4.1 Atomic absorption

The metal ion concentrations before and after the binding test were determined with an atomic absorption spectrophotometer (Perkin-Elmer, model 2380). The lamps used were also from Perkin-Elmer (Ni, M-2092; Ca, M-2453). Table 2.4 shows the characteristic wavelengths of lamps used for the analyses of the cations and other experimental parameters. The atomic absorption standard solutions were Ni, 1000 ppm (J. T. Baker Chemical Co., Phillipsburg, NJ.) and Ca, 1000 ppm (Seigniory Chemical Products Ltd., Lasalle, QC).

Table 2.4 The conditions of calibration and analysis in the determination of the concentration of cations by atomic absorption.

Cation	Wavelength (nm)	Slit (nm)	Concentration limit in linear domain (mg/L)
Ca(II)	422.7	0.7	5.0
Ni(II)	305.2	0.2	5.0

2.4.2 Choice of ions and preparation of solutions

The ion pair of Ni(II)-Ca(II) was used to simulate the industrial waste water mainly because of the ease of detection and non-interference in the atomic absorption experiments and also because of their coexistence in many waste water systems. The solutions were prepared by diluting atomic absorption standard solutions in deionized water and adjusting the pH with NaOH and HNO_3.

2.4.3 Binding tests for metal cations

The functional polymer resins tested (C3) were made by using polymerizable cosurfactants bearing an anionic group (sodium styrenesulfonate, $S\text{-}SO_3^- Na^+$), ([$S\text{-}SO_3^- Na^+$] = 0.07 M; S/DVB = 1:1 (v/v); [AOT] = 0.2 M; W = 12; size 40-60 mesh). The polymer resins were added to the various solutions of the metal cations (pH from 2 to 12, concentration from 0 to 30 ppm), stirred, and then filtered. The concentration of solution after binding was determined by atomic absorption spectrophotometry.

Binding kinetics of the metal cations. The atomic absorption standard solutions (Ca(II) and Ni(II)) were diluted to 15 ppm. The pH was adjusted to 6.0 and the total volume was 30 mL. 100 mg of polymer resins were mixed with the solution and the binding time varied from 5 to 90 minutes.

pH effect on the binding of metal cations. The concentration of cations was fixed at 15 ppm, and 15 minutes were allowed for the binding to take place. The pH of the solution was adjusted from 2 to 12. For 15 mL of the solution, 100 mg of polymer resins was used.

Concentration effect on the binding of metal cations. The pH of the solution was fixed at 6.0, and 15 minutes were allowed for the binding to take place. The concentration of the solutions was varied from 0 to 30 ppm. 100 mg of polymer resins was used for 15 mL of the solution.

3. Results and Discussion

3.1 Polymer Preparation

For the preparation of porous polymer resins, AOT was used as the surfactant to form reverse micelles in the monomer mixtures. The size of the reverse micelles was controlled by the water content W, which is expressed by the molar ratio of water entrapped in reverse micelles to AOT. Polymerizable cosurfactants were used to introduce functional groups to the resins.

Toluene is a good solvent and was used as the pore-forming reagent in the S-DVB mixture to improve the access to the smaller pores formed by reverse micelles in the polymer resins. After polymerization, the pore-forming reagent can be removed by extraction, leaving permanent pores in the polymer resins.

Three polymer resins were prepared with polymerizable cosurfactants. Two polymerizable cosurfactants with neutral group were synthesized and introduced to monomer mixture (C1 and C2). Another polymer resin (C3) was prepared by using a sodium sulfonate as cosurfactant for the binding testing. For C1 and C2, the cosurfactants were easy to dissolve in the monomer mixture and the concentration could reach 0.2 M without any phase separation at a water content W of 12. However, when the concentration of the cosurfactant was higher than 0.09 M, at W = 12, phase separation occurred for resin C3.

Two series of polymers were prepared. The first A series are polymer resins made of PMMA matrix, methyl methacrylate (MMA) as the monomer and ethylene glycol dimethacrylate (EGDMA) as the crosslinker. The second series (T-series) consists of resins made of PS matrix, with styrene as the monomer and divinylbenzene as the crosslinker.

Toluene is added as the pore-forming reagent, ranging from 0 to 60% of the total volume. The water content (W) was varied from 0 to 14. For both series of polymer resins, the concentration of AOT was fixed at 0.2 M, and W at 12.

3.2 Polymer Characterizations

3.2.1 Solid state NMR spectroscopy

As shown in the solid state ^{13}C CP/MAS NMR spectra of typical porous polymer resins based on PS matrix (Figure 3.1), the intensities of the ^{13}C NMR signals due to the aliphatic chains of the surfactant AOT (10-35 ppm) (Figure 3.1A) are much diminished after washing (Figure 3.1B). The spectrum of the polymer resin after washing (Figure 3.1B) is the same as that of a polymer made without any surfactant (Figure 3.1C). The NMR spectra show that most AOT molecules have been successfully extracted from the ground polymer resins. It may still be possible, that some residual AOT molecules were trapped in the unexposed pores inside the polymer matrix even after extensive washing. The remaining surfactants, if any, should not affect the use of the polymers because of the heavy crosslinking.

For the polymer resins based on PMMA matrix (Figure 3.2), the NMR signals of AOT were totally covered by the NMR signals of polymer matrix. The signals around 130 ppm might be those of C=C of unpolymerized monomers or crosslinkers.

3.2.2 Infrared (IR) spectroscopy

The IR spectra of a typical polymer resin made of PS matrix before and after washing are shown in Figure 3.3. It can be seen that the C=O stretching band at 1735 cm^{-1} (Figure

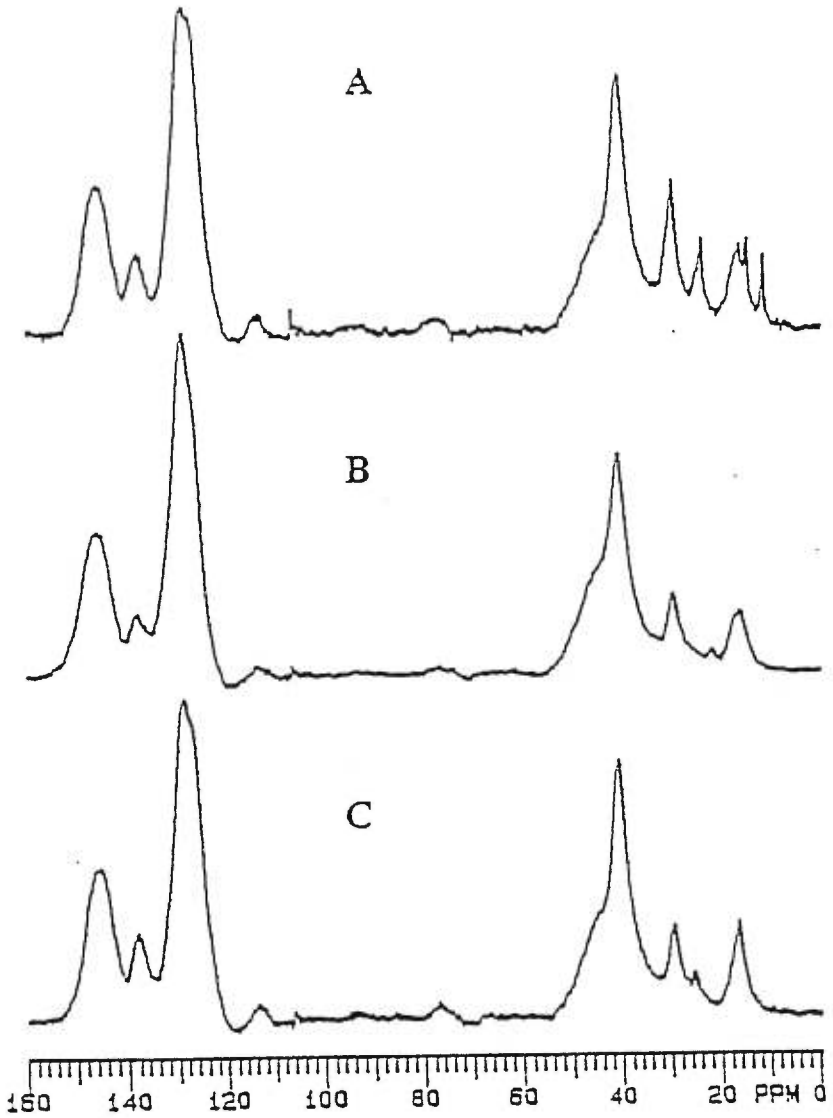

Figure 3.1 Solid state CP/MAS ^{13}CNMR spectra of polymer resins showing the effectiveness of the Soxhlet extraction: (A) a polymer resin (S:DVB = 4:1 (v/v), [AOT] = 0.2 M, W = 12) before extraction; (B) after extraction, showing the disappearance of AOT peaks from 10 to 35 ppm, which is approximately identical to (C) a poly(styrene-co-divinylbenzene) resin (S:DVB = 4:1) prepared by the same method without AOT [73].

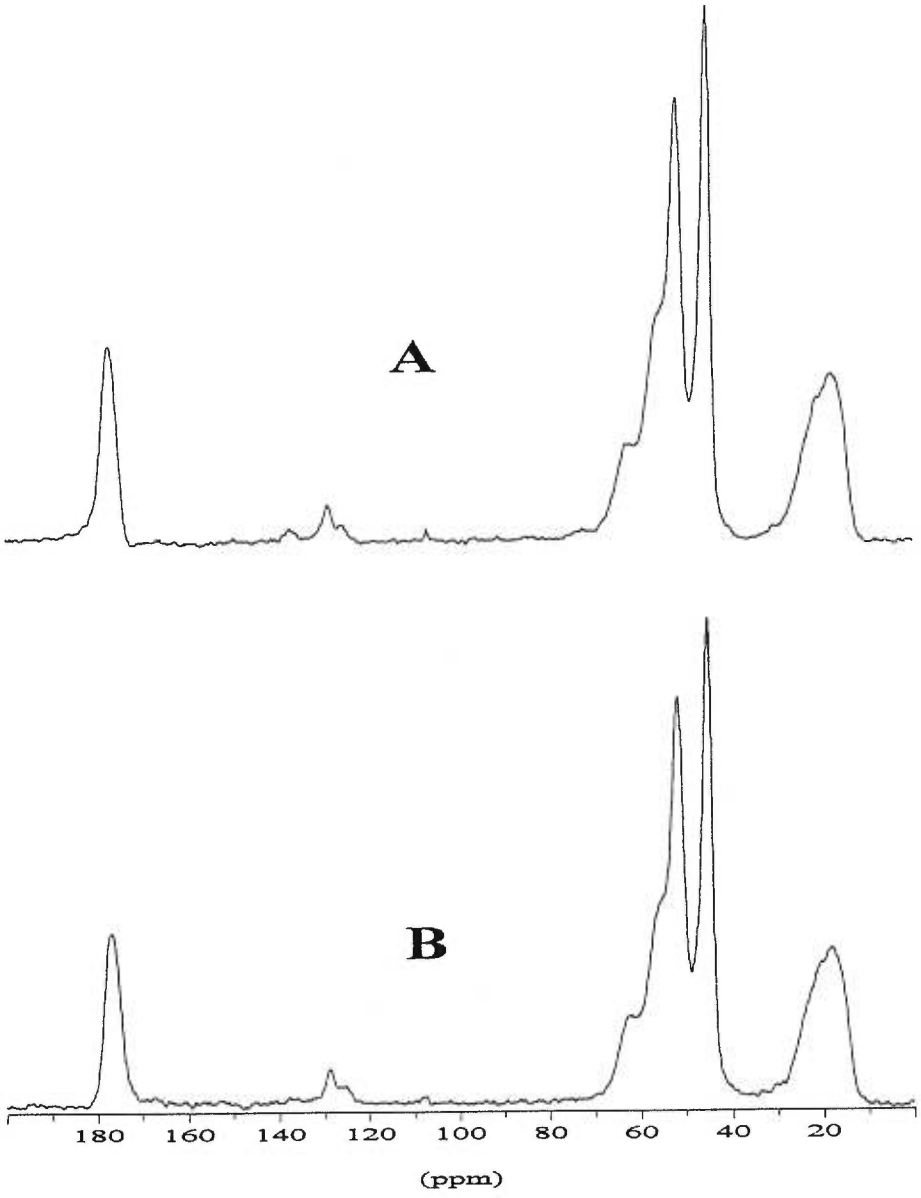

Figure 3.2 Solid state CP/MAS ^{13}C NMR spectra of polymer resins based on PMMA matrix. (A) a polymer resin (MMA:EGDMA = 4:1 (v/v), [AOT] = 0.2 M, W = 12) before extraction; (B) the same polymer after extraction.

3.3A) disappeared after washing (Figure 3.3B) along with the broader O=S=O stretching band close to 1250 cm^{-1}. Both groups belong only to the AOT molecules (Figure 1.2). The IR spectrum of the polymer after washing is comparable to that of a polymer resin made without AOT reverse micelles (Figure 3.3C). The IR spectra clearly indicate that most of the AOT molecules have been washed off during the Soxhlet extraction.

The IR spectra of the polymer resin (C2, PS matrix) prepared with polymerizable cosurfactant (6-hydroxyhexyl methacrylate) before and after washing and of a polymer resin without cosurfactant after washing are shown in Figure 3.4. In this case, both AOT and cosurfactant molecules have C=O groups, and after washing there is still C=O stretching band in the spectrum (Figure 3.4B), but the O=S=O stretching band disappeared. It indicates that the AOT molecules are removed after the extraction as usual, but the polymerizable cosurfactant molecules remained as part of the polymer matrix. Therefore, the functionalization of the polymer resin with polymerizable cosurfactant was successful.

Figure 3.5 shows that the IR spectra of a polymer resin based on PMMA matrix containing AOT before (Figure 3.5A) and after washing (Figure 3.5B). The broader O=S=O stretching band close to 692 cm^{-1} disappeared after washing, and the signal of the C=O stretching band at 1732 cm^{-1} was diminished. As AOT and MMA-EGDMA molecules all have C=O groups, the IR spectrum of the polymer after washing was subtracted from the spectrum of the polymer before washing, the result is shown in Figure 3.5C. The main differences between two spectra are the C=O stretching band and the O=S=O stretching band belonging to the AOT molecules. It clearly indicates that the AOT molecules in the polymer resin made by PMMA matrix have been washed off during the Soxhlet extraction.

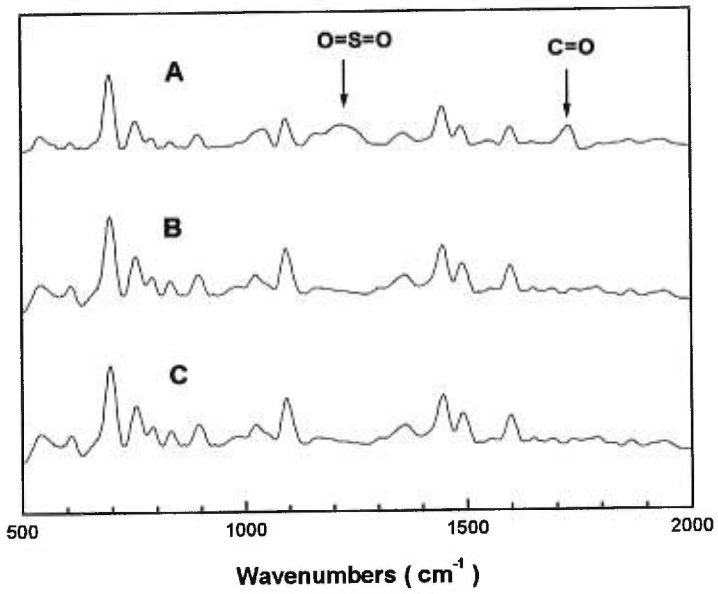

Figure 3.3 IR spectra of a polymer resin ([AOT] = 0.2 M, W=12, S:DVB = 1:1, v/v) before (A) and after (B) Soxhlet extraction, showing the disappearance of the C=O stretching band at 1735 cm^{-1} belonging to the AOT molecules after washing. (C) IR spectrum of a nonporous polymer resin made without AOT reverse micelles (S:DVB =1:1, v/v).

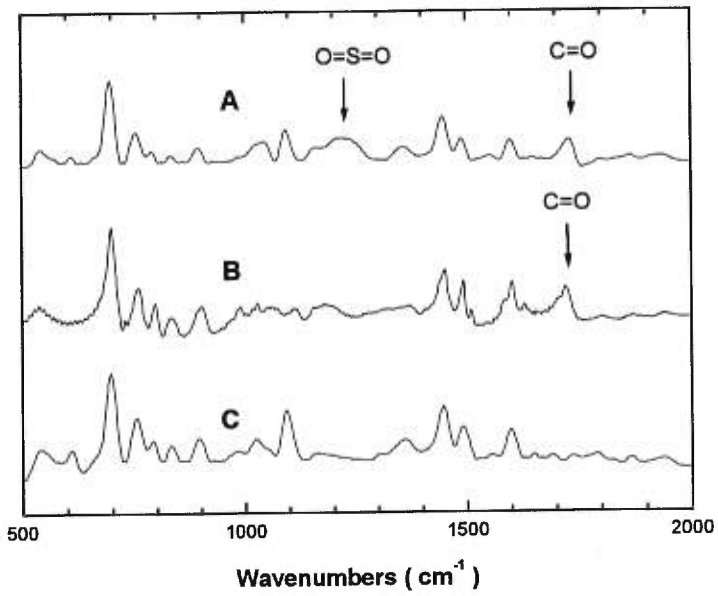

Figure 3.4 IR spectra of a polymer resin (C2, [AOT] = 0.2 M, W = 12, [ROH] = 0.2 M, S:DVB = 1:1, v/v) prepared with a polymerizable cosurfactant (6-hydroxyhexyl methacrylate) before (A) and after (B) the Soxhlet extraction, showing the disappearance of the O=S=O stretching band at 1250 cm^{-1} belonging to the AOT molecules after washing, but the polymerizable cosurfactants remained; (C) IR spectrum of a polymer resin made with AOT reverse micelles without any cosurfactants ([AOT] = 0.2 M, W = 12, S:DVB =1:1, v/v).

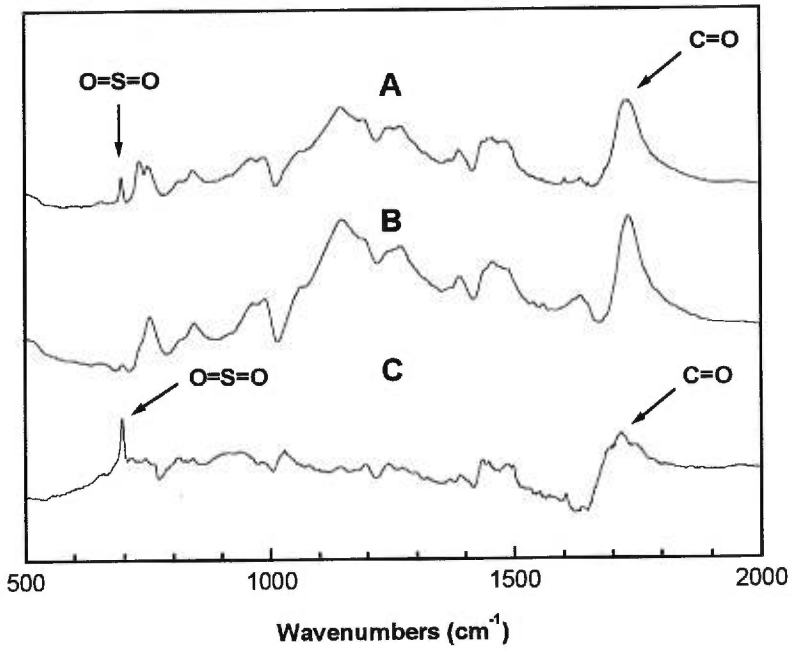

Figure 3.5 IR spectra of a polymer resin based on PMMA matrix (MMA:EGDMA = 4:1, (v/v), [AOT] = 0.2 M, W = 12) before (A) and after (B) Soxhlet extraction. The IR spectrum of the polymer after washing was subtracted from the spectrum of the polymer before washing, the result (C) showing the main differences are the O=S=O stretching band and the C=O stretching band which belonging to AOT molecules.

3.3 Gas Adsorption Experiments

The BET gas adsorption experiments were performed to determine important parameters such as the surface area, the pore volume, the cavity size, and the distribution of the cavity sizes in the polymer resins.

3.3.1 Adsorption and desorption isotherms

Figure 3.6 shows the adsorption and desorption isotherms of nitrogen on polymer resins. Both polymer resins were prepared with PMMA matrix, as described previously (Section 2.2.2). These two curves are type IV isotherms according to the IUPAC classification, and the hysteresis loops belong to the H3 type, which is associated with capillary condensation in mesopores. The ascending curve describes progressive adsorption of the N_2 gas in the system, and the descending one shows the gas evaporation. The adsorption and desorption curves are not overlapped, a characteristic of mesoporous solids.

At low pressures, the adsorption isotherm follows a type 2 behavior, which indicates that the gas molecules are adsorbed on the surface of polymer resins through a monolayer or multilayer process. At higher pressures, the deviation from linearity shows mesopores of polymer were filled when the saturation vapor pressure was approached.

The adsorption and desorption isotherms of a non-porous polymer resin are shown in Figure 3.6B. This polymer resins is an MMA-EGDMA-based copolymer prepared without AOT and water. For this non-porous material, the amount of gas adsorbed is very small and no significant difference of two isotherms can be observed. The surface area of this polymer as determined by the BET method is very small (0.1 m^2/g). When the material is porous, the

adsorption and desorption isotherms do not overlay because of the porous structure of the material (Figure 3.6A), and the surface area (21.8 m^2/g) is much large.

Some polymer resins were prepared in aluminum plates. The loss of the monomer mixture by evaporation during the polymerization process can be quite significant, sometimes as high as 20% by weight. The concentration of AOT, the water content, and the degree of crosslinking become hard to control. To improve the procedure, the mixture was placed to an ampoule, which was then sealed to avoid the possible loss of the monomers. As soon as the liquid monomer mixture became solid, the mixture was transferred in an oven and heated up to 70 °C overnight. The adsorption-desorption hysteresis loops of two polymer resins prepared with the different procedures are shown in Figure 3.7. The specific surface area of the porous polymer resin increased from 12.8 m^2/g to 32.1 m^2/g when a sealed ampoule was used.

To further expose the functional cavities of the resins, toluene, a good solvent of the monomer mixture, was added as the pore-forming reagent. Figure 3.8 illustrates the improvement of surface area of polymer resin by using the pore-forming reagent during the preparation of the resins. The surface area of the polymer resin prepared with toluene is much higher (77.0 m^2/g) than a porous resin made without any porogenic agents (30.3 m^2/g). The details of the effect of the pore-forming reagent will be discussed in Section 3.3.5.

3.3.2 Determination of specific surface with BET and Langmuir method

The specific surface area of the polymer resins can be calculated from the adsorption-desorption isotherms with the BET equation. (Section 1.4.2)

Figure 3.9 shows the plot of $P/[V(P_0-P)]$ as a function of P/P_0 for a polymer resin

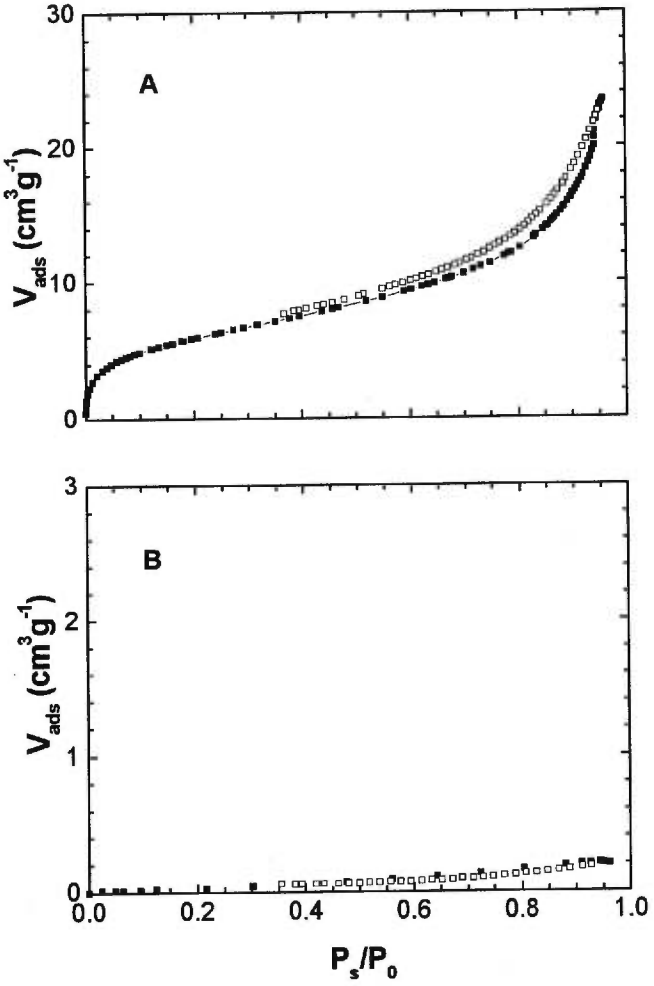

Figure 3.6 BET adsorption (closed symbols) and desorption (open symbols) isotherms of polymer resins made with PMMA matrix (MMA:EGDMA = 4:1, v/v). (A) porous polymer; [AOT] = 0.2 M, W = 6, (B) a non-porous resin.

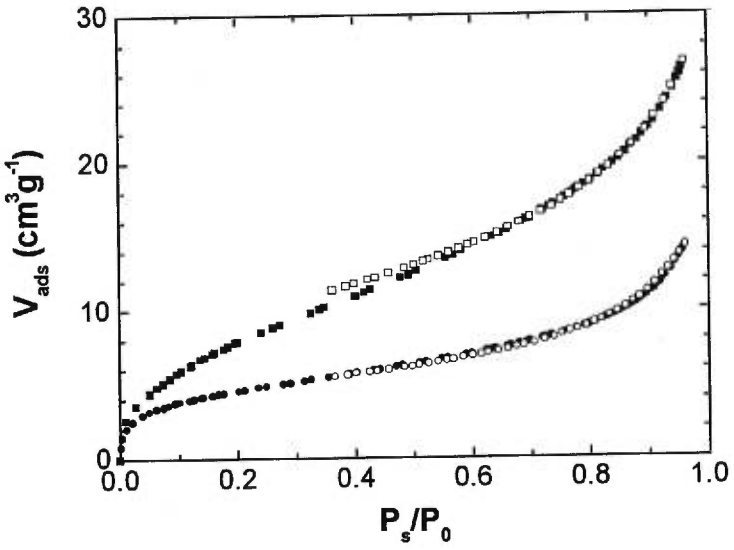

Figure 3.7 BET adsorption and desorption isotherms of two porous polymer resins; [AOT] = 0.2 M, W = 12, S:DVB = 1:1, v/v. Square, Resin made in a sealed ampoule; circles, Resin made in an open ampoule. Closed symbols, adsorption curves; open symbols, desorption curves.

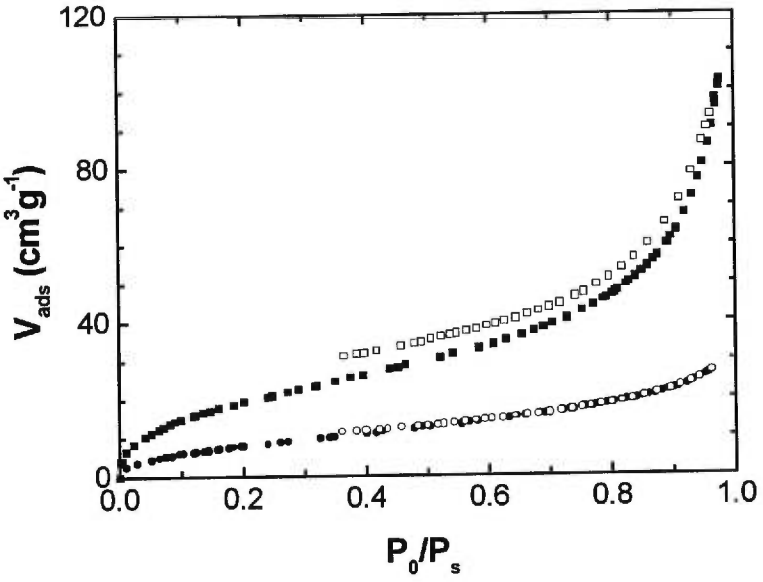

Figure 3.8 BET adsorption and desorption isotherms of porous polymers prepared with PS matrix; [AOT] = 0.2 M, W = 12, S:DVB = 1:1, v/v. Squares, polymer resin made with pore-forming reagents, [Toluene] = 50 %, v/v. Circles, polymer resin without toluene. Closed symbols, adsorption curves; open symbols desorption curves.

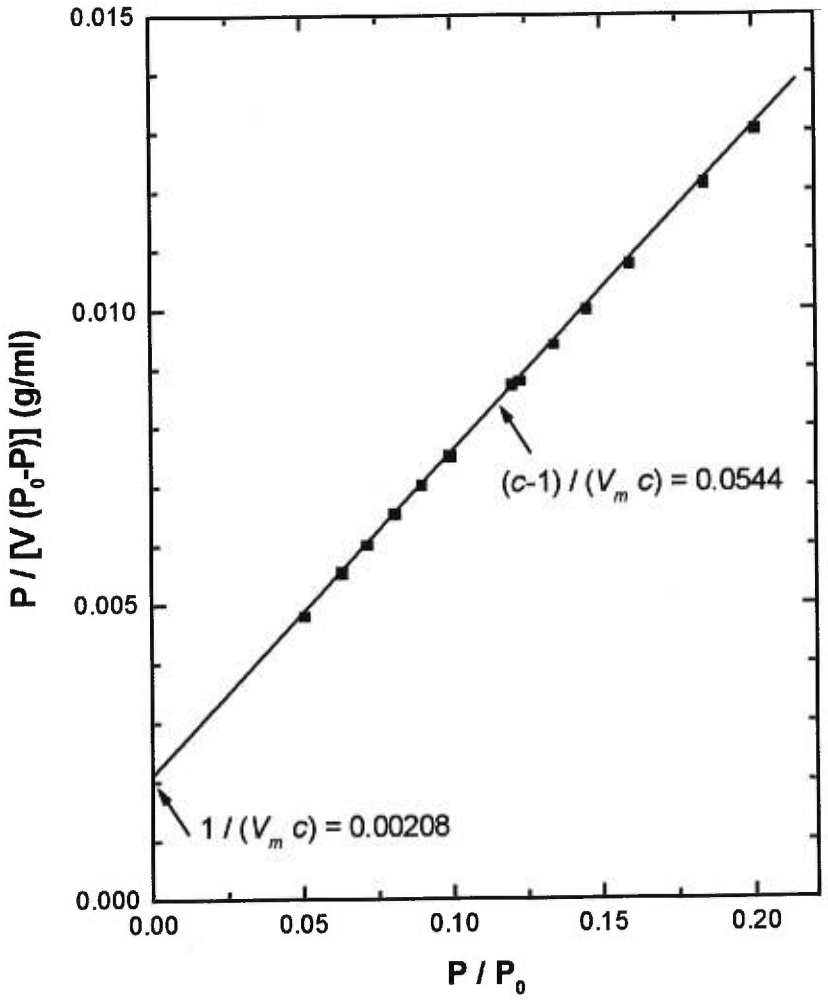

Figure 3.9 The BET plot of a porous polymer resin. [AOT] = 0.2 M, W = 12, [Toluene] = 50 vol%. The monolayer volume (V_m = 19.113 mL) and the BET constant (c = 25.154) can be obtained from the intercept and the slope of the plot.

prepared with PS matrix and toluene as the pore-forming reagent. From the slope $(c\text{-}1)/(V_m c)$ (0.0544) and the intercept $1/(V_m c)$ (0.00208), the monolayer capacity V_m is calculated to be 17.7 cm^3/g, and the BET specific surface area is 77.0 m^2/g.

3.3.3 Determination of the pore size distribution with the BJH method

The detail of BJH method was introduced in Section 1.4.3. The use of the BJH method to determine the pore size distribution of the polymer resins is discussed here.

An application of this procedure is given in Table 3.1 and the pore volume distribution curves of polymer resin (C3) obtained from the adsorption and desorption isotherms are shown in Figure 3.10.

The pore size distribution curves are plots of the volume increment ($\Delta V/\Delta D$) as a function of pore diameter (D) obtained either from the desorption or adsorption isotherms. The maxima of the two distribution curves indicate the respective pore size at which there is the largest pore volume increment. For resin C3, the pore size distribution calculated from the desorption isotherm is narrower, and the diameter with maximum volume increment (D_{mv}) and the average diameter (D_{av}) are different from the values obtained from the adsorption isotherm (Figure 3.10). The reason of this difference is still not very clear and there are no general recommendations for the selection of hysteresis loop [64]. It is important to choose systematically one of the isotherms for the comparison on the result. For all polymer resins in this study, the pore diameters were determined from the adsorption isotherms.

Table 3.1 Evaluation of pore size distribution with the BJH model.

Relative pressure P_s/P_0	Volume desorbed V_D (cm^3g^{-1})	Condensed volume V_c (cm^3g^{-1})	Core radius r_c ($\times 10^{-10}$ m)	Residual thickness t ($\times 10^{-10}$ m)	Pore thickness r_p ($\times 10^{-10}$ m)	$\bar{r}_c$	r_p	Δt	ΔV_c (cm^3g^{-1})	ΔV_p (cm^3g^{-1})	ΔS_p (m^2g^{-1})	Δr_p ($\times 10^{-10}$ m)	$\Delta V_p/\Delta r_p$ ($cm^3m^{-1}g^{-1}$)	$\Delta S_p/\Delta r_p$ ($cm^3m^{-1}g^{-1}$)
0.99	220	0.3403	939.0	19.1	958.0									
0.95	203	0.3140	184.0	15.8	200.0	562	579	3.33	0.0263	0.0279	0.96	758.0	0.4	0.01
0.90	193	0.2986	89.6	13.2	103.0	137	151	2.52	0.0154	0.0185	2.45	97.0	1.9	0.3
0.85	184	0.2846	58.0	11.6	69.6	74	86	1.68	0.0140	0.0183	4.25	33.6	5.4	1.3
0.80	174	0.2692	42.2	10.3	52.5	50	61	1.23	0.0154	0.0214	7.03	17.1	12.5	4.1
0.75	164	0.2531	32.8	9.4	42.2	38	47	0.96	0.0161	0.0234	9.89	10.3	22.7	9.6
0.70	151	0.2336	26.5	8.6	35.1	30	39	0.78	0.0195	0.0297	15.40	7.1	41.8	21.7
0.65	138	0.2135	22.0	8.0	30.0	24	33	0.65	0.0201	0.0313	19.30	5.1	61.4	37.8
0.60	124	0.1918	18.5	7.4	25.9	20	28	0.56	0.0217	0.0351	25.10	4.1	85.6	61.2
0.55	111	0.1709	15.8	6.9	22.7	17	24	0.49	0.0209	0.0338	27.80	3.2	105.6	86.9
0.50	97	0.1501	13.6	6.5	20.1	15	21	0.44	0.0208	0.0336	31.40	2.6	129.0	121.0
0.45	84	0.1299	11.8	6.1	17.9	13	19	0.40	0.0202	0.0323	34.00	2.2	146.8	154.5
0.43	79	0.1222	11.2	5.9	17.1	12	18	0.15	0.0077	0.0116	13.30	0.8	145.0	166.3
0.40	75	0.1162	10.3	5.7	16.0	11	17	0.22	0.0062	0.0020	2.44	1.1	18.2	22.2
0.35	70	0.1085	9.0	5.3	14.3	10	15	0.35	0.0077	0.0051	6.80	1.7	30.0	40.0
0.30	66	0.1019	7.8	5.0	12.8	8	14	0.33	0.0066	0	0	1.5	0	0

$v_c = 1.547\times10^{-3}\, v_D$; $t^2 = 13.99 / (0.034 - \log x)$; $r_P = r_c + t$; $r_c = r_k = -4.1 / \log x$, x equal P_s/P_0.

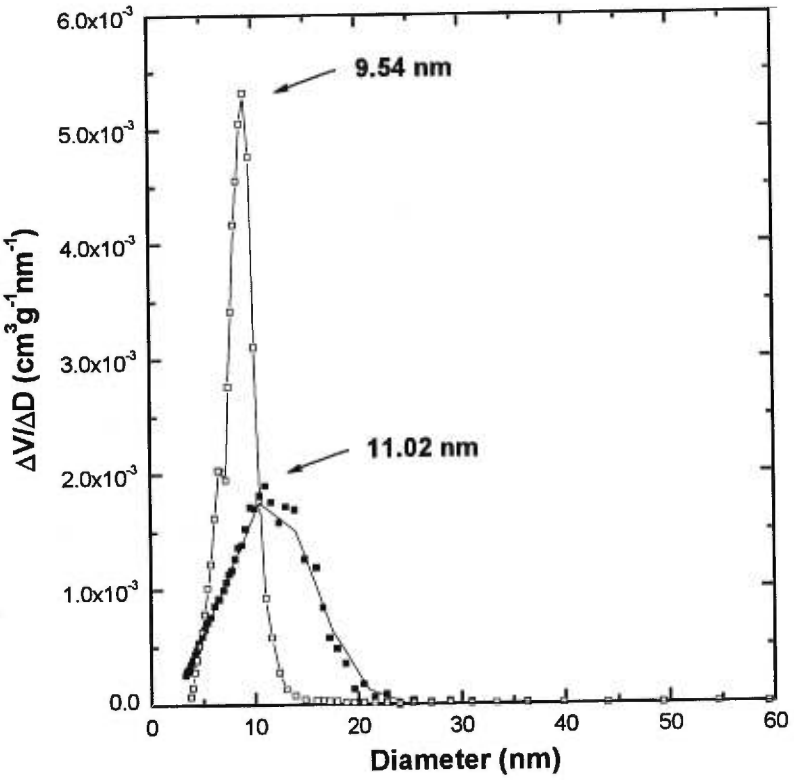

Figure 3.10 Distribution of pore diameters obtained from adsorption (closed symbols) and desorption (open symbols) isotherms of the polymer C3. [AOT] = 0.2 M, [S-$SO_3^-Na^+$] = 0.07 M, W = 12, S:DVB = 1/1 (v/v), mesh size 40-60 (particle size 250-425 μm).

Calculation of Average pore diameter

The average pore diameter can be calculated with the BJH method and cylindrical pore model. The calculation is based on two assumptions: (a) the pore volume of micropores is small, and can be ignored; (b) the length of all pores with different diameters is constant or can be calculated from pore diameters.

From the BJH method, we can obtain the volume of the pores of a certain diameter range. When we assume that the pores are cylindrical and the length of the pores is known or can be calculated, the number of pores of a certain diameter range can be calculated. Then, the average pore diameter (D_{av}) can be determined.

The average pore diameter (D_{av}) can be calculated by

$$D_{av} = \frac{\sum_i n_i D_i}{\sum_i n_i} \tag{3.17}$$

where n_i is the number of the pores with a certain diameter of D_i. From the cylindrical pore model,

$$V_i = n_i \pi \ D_i^2 L_i \tag{3.18}$$

where, V_i total pore volume of the pores with a diameter of D_I, L_i is the length of these pores.

If we assume that all the pores with various diameters have the same length L, we can define the average pore diameter as

$$D_{av} = \frac{\sum_i V_i / D_i}{\sum_i V_i / D_i^2}. \tag{3.19}$$

For a special case where the length of pores L_i equals pore diameter, $L_i = D_i$, Equation 3.18 becomes

$$D_{av} = \frac{\sum_i V_i / D_i^2}{\sum_i V_i / D_i^3}. \qquad (3.20)$$

If we assume that the length of all pores is the same, D_{av} is very close to the diameter with maximal volume increment (D_{mv}) on the distribution curve. If we assume that $L_i = D_i$, however, the D_{av} value is much larger. Therefore, the first assumption seems to be closer to reality and is thus used for the calculation of the D_{av}-values of the resins. Table 3.2 shows the results from BET gas adsorption experiment.

Table 3.2 Specific surface area, total pore volume and average diameter from BET gas adsorption experiment.

Resin	S_{BET} (m^2/g)	V_{total} (mL/g)	D_{av} (nm)
C1	24.3	0.064	17.6
C2	17.4	0.051	11.6
C3	18.6	0.047	12.9

3.3.4 Variation of water content (W) (PMMA matrix)

A new series of porous polymer resins with PMMA-based matrix was prepared in comparison with the resins with PS matrix. In this series, the concentration of AOT was fixed at 0.2 M and the water content in the AOT reverse micelles was varied.

Figure 3.11 illustrates the variation of BET specific surface area, volume, and average pore diameter (D_{av}) as a function of water content W of these polymer resins. The BET specific surface areas, pore volume and average diameter increase with water content W and

reach a plateau at high W. For this series of polymer resins, when the water content W reached beyond 10, the mixture was no longer homogeneous. Thus a phase separation occurred during the preparation.

The pore size of these polymer resins changed gently in this water content range (W from 2 to 10) when compared with the polymer resins based on PS matrix [73]. It may be due to the effect of different monomer and crosslinker. Methyl methacrylate is more polar than styrene, and in our case the crosslinker content was quite high (Chieng *et al.* used only 4 wt% of EGDMA as crosslinker) [77]. These factors may affect the formation of AOT reverse micelles. At low W, the phase separation was not observed, but the solubilization of water was not very easy. At high W (beyond 10), the mixture becomes cloudy indicating the occurrence of phase separation clearly occurred, and the pore size could not be controlled by the water content in reverse micelles. At low W values, the pores were created by the reverse micelles. From the adsorption and desorption isotherms, the existence of mesopores was clear.

3.3.5 Effect of pore-forming reagent

The polymers were ground into fine particles to ensure the exposure of the functional cavities inside the resins during the binding. Extra fine particles may slow down the flow and are not desirable for many applications. To increase the accessibility of the pores, additional pore-forming reagents may be added during the preparation of the polymers. The AOT reverse micelles are dispersed in the mixture of the monomer, crosslinker and a non-polymerizable pore-forming reagent. After polymerization, this reagent is washed off together with the micellar templates during the extraction. This will leave the polymer resin

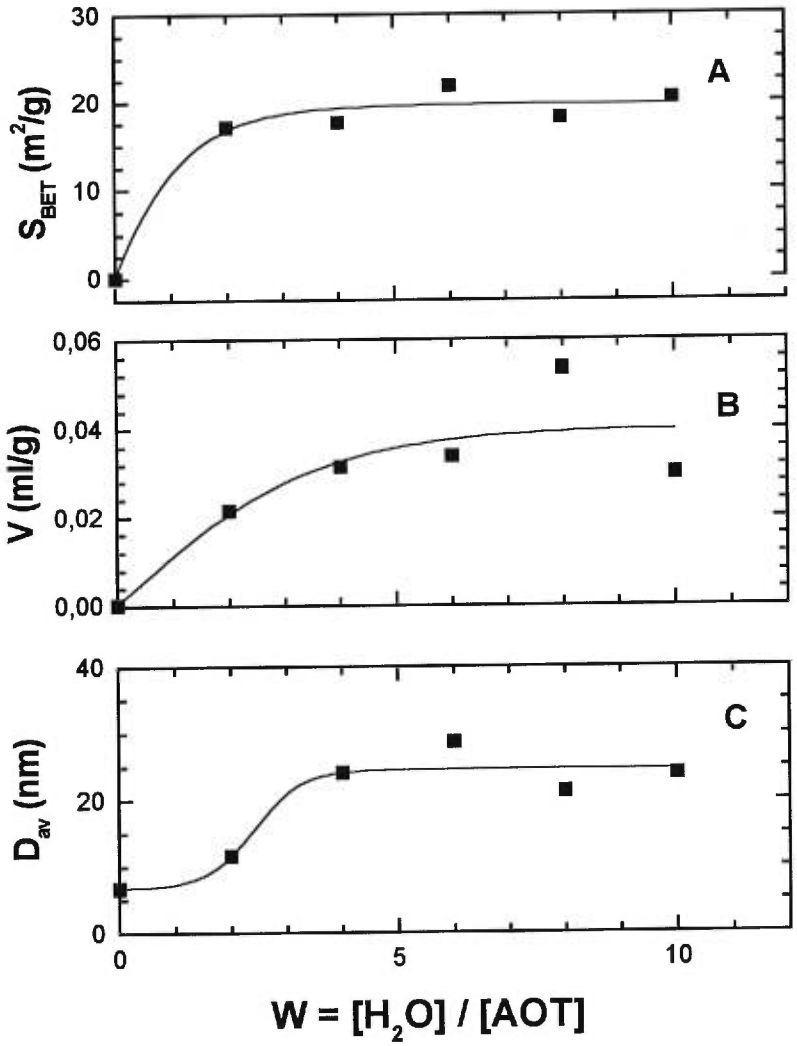

Figure 3.11 Variation of BET specific surface area (A), total pore volume (B) and average diameter of the pores (C) as a function of water content in reverse micelles. Polymer resins with varying W: MMA:EGDMA = 4:1 (v/v), [AOT] = 0.2 M.

with large channels giving access to the well-defined smaller pores formed by the micellar templates (Figure 2.2). This will ensure a better accessibility of the cavities of the resins.

A series of S-DVB resins with toluene as the pore-forming reagent were prepared. As shown in Figure 3.12A, the surface area increased from ca. 30 m^2/g to almost 80 m^2/g. Figure 3.12 represents the variation of BET surface area, total pore volume, and pore size as a function of the amount of pore-forming reagent used. We can notice that both specific surface area and total pore volume increase linearly as a function of the volume fraction of toluene used. The pore size (average diameter of the pores) also shows an increase with the toluene content.

The cavities in these porous resins consist of well-defined pores formed by AOT reverse micelles and irregular pores by pore-forming reagents. As the concentration of AOT and water content are constant, the increase of surface area and pore volume is mainly contributed by toluene. The average pore diameter is obtained by the BJH method, which assumed all the pores were cylindrical, but the pores from toluene had irregular shape. Therefore, the average pore diameter is a simplified result but it still shows an increase with the addition of toluene (Figure 3.12C). At higher toluene content, the change was not very significant.

The study of the effect of pore-forming reagents on porous resins made with AOT reverse micelles is still preliminary. A lot of interesting aspects still need to be investigated, such as the addition of other pore-forming reagents, the distribution of two kind of pores, how the amount of pore-forming reagents affects the binding properties and stabilities of the porous structure of the polymers.

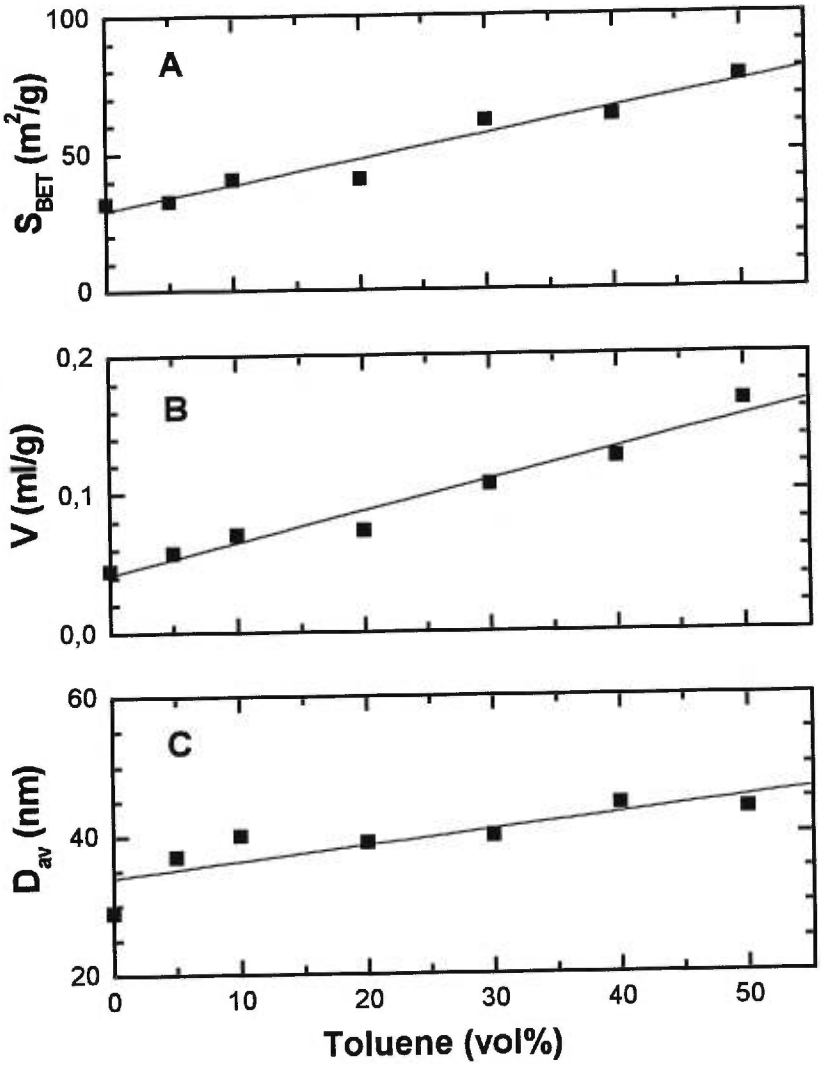

Figure 3.12 The BET specific surface area (A), total pore volume (B) and average pore size (C) plotted as a function of the amount of pore-forming reagent (toluene) used in the monomer-crosslinker mixture. Polymer resins with varying amount of toluene as pore-forming reagent: S:DVB = 1:1 (v/v), [AOT] = 0.2 M.

3.4 Test of binding of metal cations with functionalized polymer resins

To study the selective binding of metal cation pairs, the polymer resin (C3) with anionic functional groups ($-SO_3^-Na^+$) was used. The total pore surface area and pore volume as well as the average pore diameter were determined by BET gas adsorption experiments. The result for three different resins are given in Table 3.2, and the examples of the distribution curves of the cavity sizes have been shown in Figure 3.11. No significant differences are observed among the three resins. But the three parameters listed for resin C1 are consistently higher than those of the other two resins. This may be due to that the cosurfactant used for C1 resin 6-(*p*-vinylbenzyloxy)hexanol is less polar than the other two cosurfactants. The particle size is fixed between 40 to 60 mesh (250-425 μm) in order to allow the diffusion of the solution and to maintain a reasonable flow rate. The BET gas adsorption experiments indicate an average pore diameter of C3 of around 13 nm, that is much larger than the diameter of the cations. Therefore, both Ca(II) and Ni(II) can have sufficient interactions with the resins.

We have tested the resins by adding them to the cation solutions, followed by stirring and filtration. The stirring time is the time allowed for the binding to take place. The optimal time was determined by a kinetic study, as described in Section 2.4.2.

3.4.1 Binding kinetics

The rate of ion-exchange is important in system design. Metal cation pairs can be separated by the difference of their sorption rates on a resin in a dynamic system. A kinetic study can help to determine the optimal time in the binding process. For industrial cation-exchange resins, high exchange rates and high binding capacities are required.

For a column system, the flow rate of the eluent affects significantly the amount of cations bound. When the flow rate of eluent and the diffusion of solutes in the resins is rapid, the contact time between the solute and the resins is short. In the stirring of the binding mixture, the stirring time was controlled instead of the flow rate of the eluent.

Figure 3.13 presents the quantity of adsorbed cations from a mixture of Ca(II)-Ni(II) as a function of stirring time. The pH was fixed at 6.0, and the concentration was 15 ppm for each cation in both individual and competitive binding experiments. As shown in this figure, in both individual or competitive bindings, the binding capacity for Ni(II) is higher. In the individual binding of the cations, both reached an equilibrium within about 20 minutes. In the competitive binding, for Ca(II) cation, the adsorbed quantity almost reached the saturation level after 10 minutes of stirring, but for Ni(II) cation, the plateau was reached after ca. 25 minutes. However, the binding capacity for Ni(II) cation is much higher than for Ca(II) under the same conditions (competitive binding). This porous polymers can bind more Ni(II) than that Ca(II) at pH 6.0, if the time allowed for the interaction is long enough. But when it is short, the adsorbed quantities of both Ca(II) and Ni(II) cations may be quite close, which will not allow an easy separation of the pair.

The binding capacity of polymers for Ni(II) cation is much higher than for Ca(II), since the ionic radius of Ni(II) is smaller and the charge density is higher, making the ionic interactions stronger (Table 3.3).

In general, both Ca(II) and Ni(II) cations are hydrated with 6 water molecules ($[M(H_2O)_6]^{2+}$). As shown in Table 3.4, the bare ionic radius of Ca(II) is larger than that of Ni(II). But the real hydrated ionic radius should be different. The results of kinetic studies still show that Ca(II) cation is bound to a lesser extent than Ni(II) at pH 6.0.

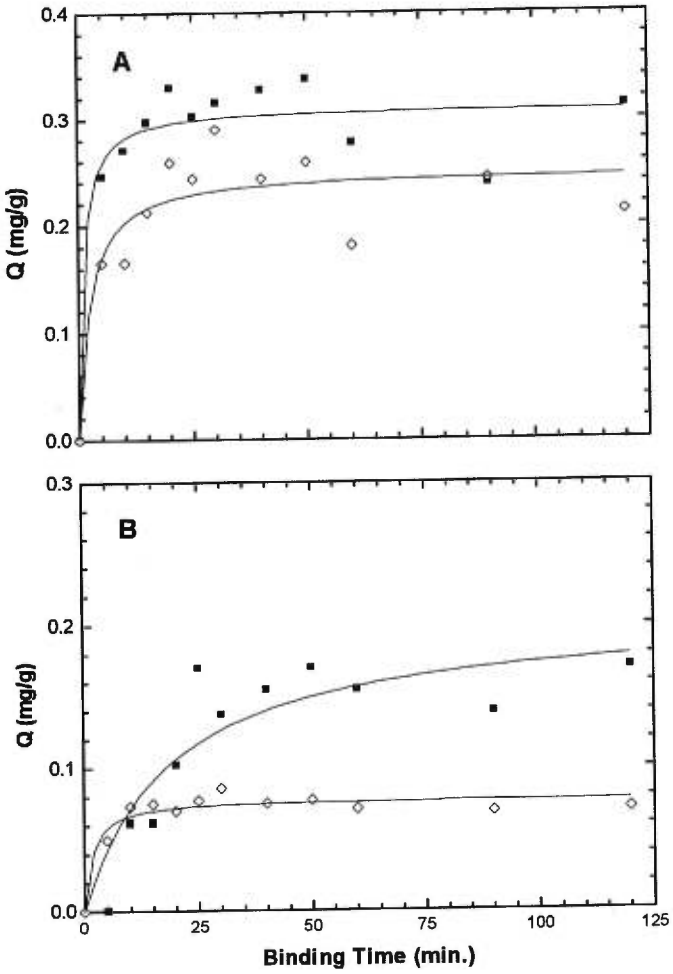

Figure 3.13 Quantity of the bound Ca(II) (diamond symbols) and Ni(II) (square symbols) cations as a function of stirring time in the solution of cations at pH 6 (A: individual binding; B: competitive binding). The polymer resin used (C3): S:DVB = 1:1, [AOT] = 0.2 M, W = 12, [S-SO^{3-} Na^{+}] = 0.07 M, mesh size 40-60 (particle size d = 250-425 μm).

Table 3.3 The hydration enthalpy, ionic radius of Ca(II) and Ni(II)

Cation†	Hydration enthalpy (kJ mol^{-1})	Bare ionic radius (Å)
Ca(II)	-1577	1.14
Ni(II)	-2105	0.69

(† The coordination numbers of the ions is 6. ‡ At 298 K, in water) [63,76]

3.4.2 pH effect

In the binding process, the interactions depend on the dissociation constants in the equilibrium and on binding kinetics. It is well known that ion exchange may be influenced by the pH of the solution. The hydration state of the cations in water may also be affected by the pH.

Figure 3.14 illustrates the difference of the binding of two metal cations, Ca(II) and Ni(II) with a polymer resin when pH changed from 2 to 12. A maximum binding peak is observed for each metal cation as a function of pH; the maximum binding for Ca(II) and Ni(II) occurred at ca. pH 6 and 8, respectively. Hence the metal cation pairs may be separated by adjusting the pH of the solution.

At a higher pH, there are more OH^- anions, the ion-exchange process may be in competition with another chemical equilibrium and the ionic complex may exist as $(M(H_2O)_{6-x}(OH)_x^{2-x})$:

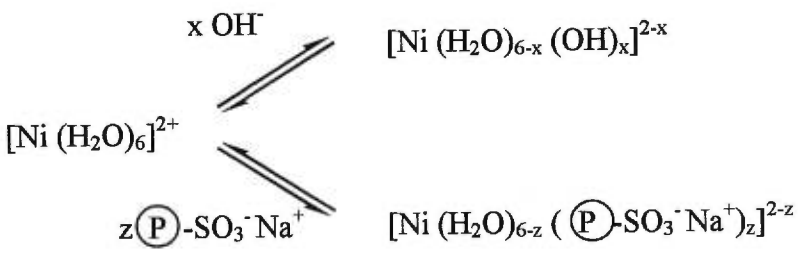

(3.21)

Therefore, the pH of the solution may be quite important in the binding. At high pH, the OH^- anion may form complexes with the metal cations, which makes the binding of cations also difficult. At low pH, the NO_3^- anion may also form complexes with cations. The difference in the sorbed quantities can be attributed to the different affinities between the sulfonate group and the hydrated metal cations. As shown in Figure 3.14, the effect of pH in either competitive binding or individual binding is about same.

3.4.3 Concentration effect

The concentration of metal cations in a solution is important in the ion-exchange process. The ion-exchange process is a chemical equilibrium.

$$M^{2+} + \text{Ⓟ}\text{-}SO_3 \underset{}{\overset{K}{\rightleftharpoons}} M[\text{Ⓟ}\text{-}SO_3]_2 \qquad (3.22)$$

The equilibrium constant (K) can be written as

$$K = \frac{[M^{2+}(P-SO_3)_2]}{[M^{2+}][P-SO_3]^2}. \qquad (3.22)$$

Assuming a homogenous distribution of the functional groups ($-SO_3^-Na^+$) in the polymer resins, their number per unit mass of polymer resins is fixed, and thus the concentration of active centers in the polymer resins is fixed too. Therefore, the ion-exchange equilibrium just depends on the concentration of metal cation. And this ion-exchange equilibrium can be described with the Langmuir equation (Equation 1.5). In this case, the Langmuir also can be written as

$$Q = \frac{Q_m K C_{eq}}{1 + K C_{eq}}. \qquad (3.24)$$

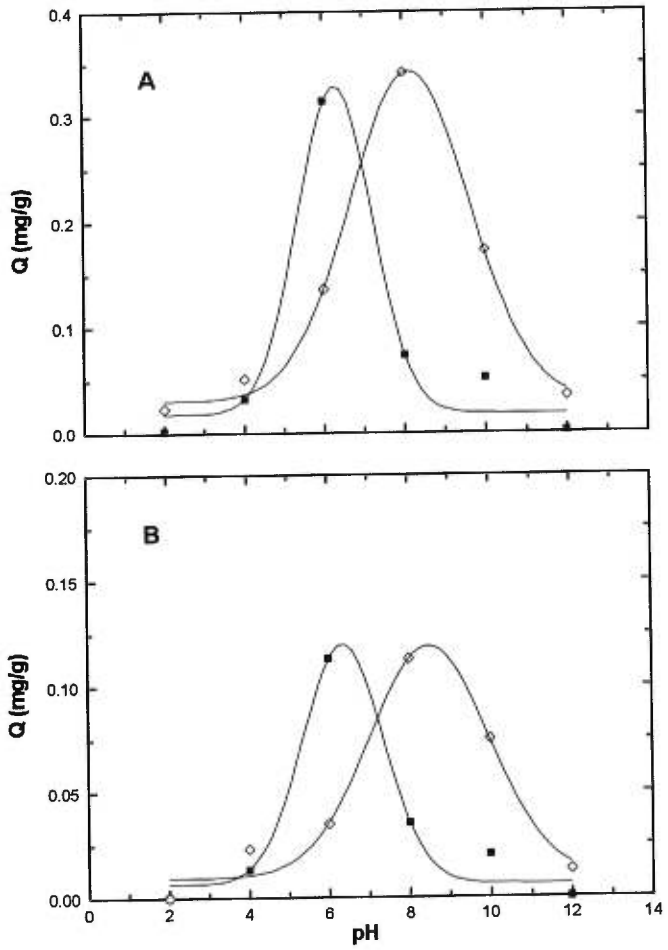

Figure 3.14 The binding capacity of Ca(II) (diamond symbols) and Ni(II) (square symbols) as a function of pH of the solution of the cations (A: individual binding; B: competitive binding). Polymer resin used (C3): S:DVB = 1:1, [AOT] = 0.2 M, W = 12, [S-$SO^{3-}Na^{+}$] = 0.07 M, mesh size 40-60 (particle size d = 250-425 μm).

where Q_m maximum binding capacity for the cations, K the ion-exchange equilibrium constant, C_{eq} equilibrium concentration of metal cations. Table 3.4 shows the results from the Langmuir equation for both individual and competitive bindings.

Table 3.4 The coefficients of the ion-exchange equilibrium from the Langmuir equation.

	Individual binding		Competitive binding	
	Ni(II)	Ca(II)	Ni(II)	Ca(II)
Q_m (mg/g)	0.34	0.23	0.17	0.07
K (L/mol)	22.89	6.01	24.65	6.41

The ion-exchange equilibrium constant K does not change much for both Ni(II) and Ca(II) in individual and competitive binding. This means the ion-exchange equilibrium of two metal cations is quite independent. The maximal quantity of bound cations in individual binding shows the total ion-exchange capacity for the polymer resin C3.

As shown in Figure 3.15 the amount of cations bound increased with increasing of the concentration of cations, and the equilibrium can be fitted into the Langmuir equation curve very well. The figure shows also that at pH 6.0 the binding selectivity of this polymer resins is in the order of Ni(II) > Ca(II). The binding isotherms are similar in both competitive and individual bindings.

Compare the result of competitive binding and individual binding in all three binding study we have done, there is a significant reduction in sorption quantity (Q). This phenomenon is very interesting and unexpected, because there is not major interaction between Ca(II) and Ni(II) cations. This question should be answered in future work.

Ion-exchange is a complex process, where there are many variables. The presence of functional groups in polymer resins is most important for the interactions between the cations and polymer resins. The cavity size is obviously important in determining the binding capacity and selectivity of the cations. Detailed comparisons of the different resins with different ion pairs still need to be carried out for a better understanding of the binding of ionic species with the new porous polymer resins.

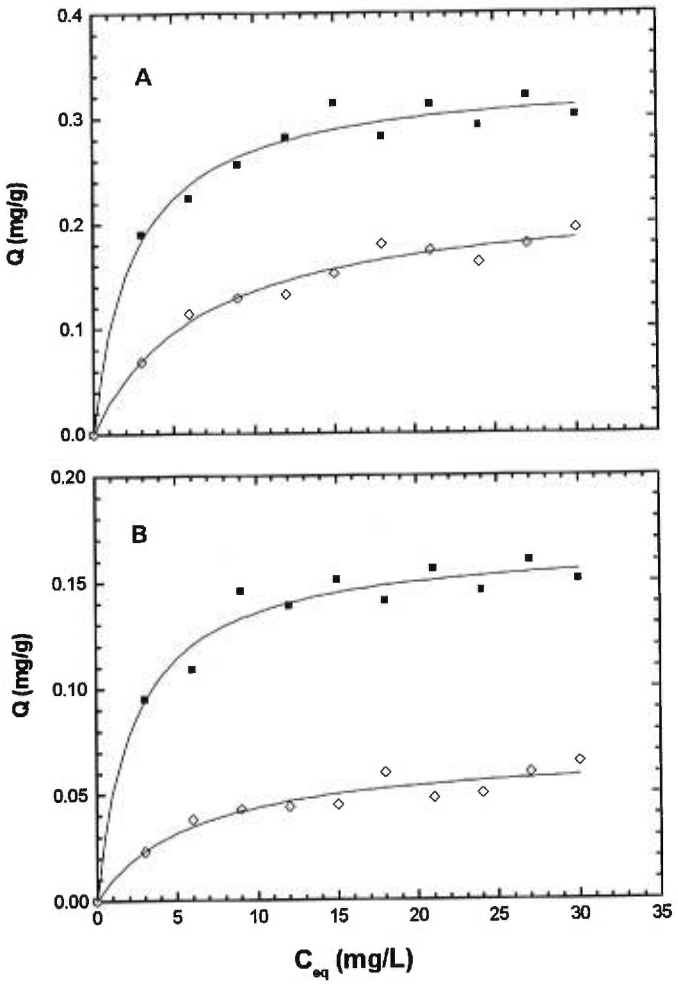

Figure 3.15 The binding capacity of Ca(II) (diamond symbols) and Ni(II) (square symbols) as a function of the equilibrium concentration of the solution of the cations at pH 6.0 (A: individual binding; B: competition binding). Polymer resin used (C3): S:DVB = 1:1, [AOT] = 0.2 M, W = 12, [S-$SO^{3-}Na^{+}$] = 0.07 M, mesh size 40-60 (particle size d = 250-425 μm).

4. Conclusion

Polymer preparation and characterization. Two series of new porous resins with well-defined cavities were prepared by polymerization in the presence of AOT reverse micelles which acted as imprinting templates. We have improved the procedure of preparation of the polymer resins by using sealed ampoules. Some polymerizable cosurfactants were synthesized and introduced into polymer resins as functional groups. The NMR and IR spectra proved the presence of the functional groups in the porous resins and the complete removal of AOT after the extraction. The functionalization process was easy, but a phase separation may occur when the concentration of cosurfactants is very high, especially for the ionic cosurfactants.

Gas adsorption experiments. All the porous polymer resins were characterized with BET gas adsorption. The specific pore surface area and the total pore volume were derived by the BET method. The average pore size and the pore size distribution were obtained from the BJH method. Our porous polymer resins are expected to provide more sharply defined exclusion limits and improved resolution in chromatographic applications. Studies on size exclusion chromatography with these resins are being carried out for a better understanding of the resins in the swollen state, and the results can be the compared with those obtained in dry state.

We have studied the effect of water content W of the AOT reverse micelles in the case MMA-EGDMA based matrices. The size of mesopores changed gently by varying W. A phase separation occurred when water content is beyond 10. Increment of the concentration surfactant or employment of other surfactant may provide improvements in

this regard. Solid state functionalization may help to overcame the phase separation problems.

To improve the accessibility of the functional cavities of the resins, toluene, a good solvent of the monomer mixture, was employed as a pore-forming reagent. We have observed that the specific surface area, total pore volume and average pore diameter all increased as a function of toluene content. For instance, the surface area increased from ca. 30 m^2/g to 80 m^2/g, which is very significant. This should be useful in the functionalization and the binding. The binding of metal cations should be more efficient with these resins.

Binding Test of metal cations. Porous polymer resins bearing negatively charged functional groups were prepared and used as ion-exchangers for selective binding of metal cations. Optimum binding conditions were assessed in the study of the binding of a metal cation pair (Ca(II) and Ni(II)). It has been shown that they can be bound selectively to the resin. The ion-exchange process is quite complex and is governed by many variables. The presence of functional groups in polymer resins is very important for the interaction between cations and polymer resins. The effect of cavity size should be important in binding of cations. The binding of others metal cations will be investigated including heavy metal ions such as Cd(II), Hg(II), Cr(II) and Cu(II), and precious metals such as Ag(I) and Au(II).

Future Work

The functionalization of polymer resins should be further investigated. New polymerizable cosurfactant can be synthesized. The solid phase synthesis may also be used to introduce functional groups into polymer resins. Other characterization techniques, such as small-angle X-ray scattering and electronic microscopy, will be used to investigate the

structure and porosity of the resins. Polymers and poor solvents can also be used as pore-forming reagents.

The shapes of the ground imprint polymer particles are irregular. Spherical beads are often desired for various applications, especially for the packing of chromatographic columns. To achieve this goal, we could use W/O/W system by dispersing the water-in-oil (W/O) mixture of monomer-crosslinker-(pore-forming reagent)-AOT reverse micelles into a continuous water media. The polymerization will take place in the resulting droplets produced by energetic stirring, and the particle size can be controlled by the stirring speed.

References

1. V. Smigol, F. Svec, J. M. J. Frechet, *Macromolecules*, **26**, 5615 (1993).
2. K. J. Shea, D. Y. Sasaki, *J. Am. Chem. Soc.*, **11**, 3442 (1989).
3. K. J. Shea, D. A. Spivak, B. Sellergren, *J. Am. Chem. Soc.*, **115**, 3368 (1993).
4. G. Wulff, p.186 in *Polymeric Reagents and Catalysts*, W. T. Ford, Ed., ACS, Washington, D. C., 1986.
5. B. Sellergren, K. J. Shea, *J. Chromotogr.*, **654**, 17 (1993).
6. F. M. Menger, T. Tsuno, G. S. Hammond, *J. Am. Chem. Soc.*, **112**, 1263 (1990).
7. F. H. Dickey, *J. Phys. Chem.*, **59,** 695 (1955).
8. R. Curti, *J. Am. Chem. Soc.*, **56**, 3961 (1952).
9. G. Wulff, A. Sarhan, *Angew. Chem., Int. Ed. Engl.*, **11**, 341 (1972).
10. G. Wulff, *Angew. Chem., Int. Ed. Engl.*, **34**, 1812 (1995).
11. K. J. Shea, *Trends Polym. Sci.*, **2**, 166 (1994).
12. J. B. Beach, K. J. Shea, *J. Am. Chem. Soc.*, **116**, 379 (1994).
13. B. Sellergren, *J. Chromatogr.*, **A 673**, 133 (1994).
14. K. Moshach., A. Li, D. J. Oshannessy, *J. Chromatogr.*, **513**, 167 (1990).
15. A. Li, B. Ekberg, K. Moshach., pp.383-394 in *Bioseparation and Catalysis in Molecularly Imprinted Polymers in Molecular Interactions and Bioseparations*, Ed. T. Ngo, New York: Plenum Press (1993).

16. K. Nilsson, J. Lindell, O. Norrlow, B. Sellergre, *J. Chromatogr.*, **680**, 57 (1994).

17. G. Vlatakis, A. Li, R. Muller, K. Mosbach, *Nature*, **361**, 645 (1993).

18. T. Dandekar, D. Argos, *Chemtracts: Biochem. Mol. Biol.*, **412**, 75 (1993).

19. H. S. Andersson, I. A. Nicholls, *Recent. Res. Devel. in Pure & Applied Chem.*, **1**, 133 (1997).

20. D. Kriz, O. Ramstrom, A. Svensson, K. Mosbach, *Anal. Chem.*, **67**, 2142 (1995).

21. D. Kriz, M. Kempe, K. Mosbach., *Sens. Actuator*, **B33**, 178 (1996).

22. K. Haupt, A. Dzgoev, K. Mosbach. *Anal. Chem.*, **70(3)**, 628 (1998).

23. O. Ramstrom, L. Ye, C. Yu, P-E. Gustavsson, *ACS Symp. Ser.* **703**, 82 (1998).

24. E. Bardez, E. Monnier, B. Valeur, *J. Phys. Chem.* **89**, 5031 (1985).

25. X. X. Zhu, K. Banana, R. Yen, *Macromolecules* **30**, 3031, (1997).

26. M. P. Pileni, *J. Phys. Chem.*, **97**, 6961 (1993).

27. K. Kurumada, A. Shioi, M. Harada, *J. Phys. Chem.*, **98**, 12382 (1994).

28. B. H. Robinson, D. C. Steyler, R. D. Tack, *J. Chem. Soc., Faraday Trans., 1*, **75**, 481 (1979).

29. M. Zulanf, H. F. Eicke, *J. Phys. Chem.*, **83**, 480 (1979).

30. J. H. R. Clarke, J. D. Nicholson, K. N. Regan, *J. Chem. Soc., Faraday Trans., 1*, **81**, 1173 (1985).

31. K. Kurumada, A. Shioi, M. Harada, *J. Phys. Chem.*, **100**, 1020 (1996).

32. M. Kotlarchyk, S. H. Chen, J. S. Huang, *J. Phys. Chem.*, **86**, 3273 (1982).

33. T. Assih, F. Larche, P. Delord, *J. Colloid Interface Sci.*, **89**, 35 (1982).

34. A. M. Ganz, B. E. Boeger, *J. Colloid Interface Sci.*, **109**, 504 (1986).

35. Y. Ikushima, N. Saito, M. Arai, *J. Colloid Interface Sci.*, **186**, 254 (1997).

36. M. P. Pileni, I. Lisiecki, M. Bjorling, L. Motte, B. Ninham, *Langmuir*, **11**, 2385 (1995).

37. M. P. Pileni, L. Motte, F. Billondet, *J. Phys. Chem.*, **99**, 16425 (1995).

38. M. P. Pileni, *Langmuir*, **13**, 3266 (1997).

39. C. Daubresse, C. Grandfils, R. Jerome, P. Teyssie, *Colloid Polym. Sci.*, **247**, 482 (1996).

40. K. Carlile, G. D. Rees, B. H. Robinson, T. D. Steer, M. Svensson, *J. Chem. Soc., Faraday Trans.*, **92**, 4701 (1996).

41. G. Cassin, S. Illy, M. P. Pileni, *Chem. Phys. Lett.*, **221**, 205 (1994).

42. A. Shioi, M. Harada, H. Rakahashi, M. Adachi, *Langmuir*, **13**, 609 (1997).

43. B. Luhmann, H. Finkelmann, G. Rehage, *Angew. Makromol. Chem.* **123/124**, 217 (1984).

44. A. Laschewsky, *Adv. Polym. Sci.*, **124**, 1 (1995).

45. K. Nagai, *Trends Polym. Sci.*, **4**, 122 (1996).

46. W. Dewinter, A. Marien, E. Michiels, *Bull. Soc. Chim. Belg.*, **99**, 977 (1990).

47. K. Nagi, H. Saton, N. Kuramoto, *Polymer*, **34**, 4969 (1993).

48. S. P. Huang, W. Li, K. J. Franz, R. L. Albright, R. H. Fish, *Inorg. Chem.*, **34**, 2813 (1995).

49. D. M. Van Berkel, D. C. Sherrington, *Polymer*, **37**, 1431 (1996).

50. W. Y. Chen, B. Z. Xu, X. D. Feng, *J. Polym. Sci.*, **20**, 547 (1982).

51. M. T. Charreyre, P. Bonllanger, C. Pichot, T. Delair, B. Mandrand, F. M. Llauro, *Makromol. Chem.*, **194**, 117 (1993).

52. Z. Gao, S. K. Varshney, S. Wong, A. Eisenberg, *Macromolecules*, **27**, 7923 (1994).

53. M. Moffit, K. Khougz, A. Eisenberg, *Acc. Chem. Res.*, **29**, 95 (1996).

54. T. Ikeda, S. Tazuke, Y. Suzuki, *Makromol. Chem.*, **185,** 869 (1984).

55. J. Seide, J. Malinsky, K. Dusek, W. Heitz, *Adv. in Polym. Sci.*, **5**, 113 (1967).

56. K. A. Kun, R. Kunin, *J. Polymer Sci.*, **A1(6)**, 2689 (1969).

57. H. Jacobelli, M. Bartholin, A. Guyot, *J. Appl. Polym. Sci.*, **23**, 927 (1979).

58. W. L. Sederel, G. J. de Jong, *J. Appl. Polym. Sci.*, **17**, 2835 (1973).

59. T. H. Chieng, L. M. Gan, C. H. Chew, S. C. Ng, K. L. Dey, *Langmuir*, **12,** 319 (1996).

60. J. Barton, *Prog. Polym. Sci.*, **21**, 399 (1991).

61. F. M. Menger, T. Tsuno, G. S. Hammond, *J. Am. Chem. Soc.*, **112**, 1263 (1990).

62. S. J. Gregg, K. S. W. Sing, *Adsorption Surface Area and Porosity*, 2nd ed., Academic Press, London, 1982.

63. P. W. Atkins, *Physical Chemistry*, 5th ed.; W. H. Freeman and Company: New York, p.986, 1994.

64. K. S. W. Sing, D. H. Everett, R. A. W. Haul, L. Mosgou, R. A. Pierotti, J. Rouquerol, T. Siemieniewska, *Pure Appl. Chem.*, **57**, 603 (1985).

65. H. Marsh, B. Rand, *J. Colloid Interface Sci.*, **33**, 101 (1970).

66. S. Brunauer, L. S. Deming, W. S. Deming, E. Teller, *J. Am. Chem. Soc.*, **62**, 1723 (1940).

67. R. Evans, U. Marini, Bettolo Marconi, P. Tazazona, *J. Chem. Soc., Faraday Trans, 2*, **82**, 1762 (1986).

68. G. Zgrablich, S. Mendioroz, L. Daza, J. Pajares, V. Mayagoitia, F. Rojas, W. C. Conner, *Langmuir*, **7**, 779 (1991).

69. A. V. Trardovski, *J. Colloid Interface Sci.*, **179**, 335 (1996).

70. D. J. Shaw, *Introduction Colloid and Surface Chemistry*, Butterworth Co., London, 1980.

71. S. Brunauer, P. H. Emmett, E. Teller, *J. Am. Chem. Soc.*, **60**, 309 (1938).

72. E. P. Barret, L. G. Joyner, P. P. Halenda, *J. Am. Chem. Soc.*, **73**, 373 (1951).

73. K. Banana, *Nouvelles résines polymères avec des pores de tailles et de formes spécifiques*, Mémoire de maîtrise, Université de Montrèal, (1996).

74. X. X. Zhu, K. Banana, H. Y. Liu, M. Krause, M. Yang, *Macromolecules*, **32**, 277 (1999).

75. M. Krause, *Résins polymères contenant des cavités polaires de grandeur définie*, Mémoire de maîtrise, Université de Montrèal, (1997).

76. F.A. Cotton, G. Wilkinson, *Advanced Inorganic Chemistry*, 5th ed. Wiley-Interscience, New York (1988).

77. T. H. Chieng, L. M. Gan, C. H. Chew, S. C. Ng K. L. Pey, *Polymer*, **37**, 4823, (1996).

78. H. F. Mark, pp. 341-393, in *Encyclopedia of Polymer Science and Engineering*, Vol. 8, 2nd ed. Wiley-Interscience, New York (1987).

79. P. H. Emmett, S. Brunauer, *J. Am. Chem. Soc.* **59**, 1553 (1937).

80. A. Zsigmondy, *Z. Anorg. Chem.* **71**, 356 (1911).

Appendix A

Physical parameters determined by BET gas absorption

A.1 Porous functional polymer resins (PS matrix) (Table 2.1)

N°	Cosurfactant (mol/L)	S_{BET} (m^2/g)	V_{total} (mL/g)	D_{av} (nm)
C1	0.20	24.3	0.064	17.6
C2	0.20	17.4	0.051	11.6
C3	0.07	18.6	0.047	12.9

A.2 Variation of water content (W) (PMMA matrix) (Figure 3.12)

N°	W=[H_2O]/[AOT]	S_{BET} (m^2/g)	V_{total} (mL/g)	D_{av} (nm)
A1	0	0.1	0.0003	6.8
A2	2	17.1	0.022	11.6
A3	4	17.7	0.032	24.1
A4	6	21.8	0.034	28.7
A5	8	18.1	0.054	21.2
A6	10	20.4	0.030	23.9

A.3 Effect of pore-forming reagent (PS matrix) (Figure 3.13)

N°	Ratio of toluene T% (v/v)	S_{BET} (m^2/g)	V_{total} (mL/g)	D_{av} (nm)
T1	0	32.1	0.045	28.9
T2	5	32.7	0.058	36.9
T3	10	40.4	0.070	40.0
T4	20	40.4	0.073	38.9
T5	30	61.4	0.106	39.8
T6	40	63.0	0.125	44.4
T7	50	77.0	0.166	43.5

Appendix B

Selective binding of metal cation pairs porous polymers

B.1 Binding kinetics (Figure 3.14)

B.1.1 The competitive binding

Time (min.)	Conc. of Ca (II) (ppm)	Q of Ca (II) (mg/g)	Conc. of Ni (II) (ppm)	Q of Ni (II) (mg/g)
0	15.00	0	0	0
5	14.83	0.050	15.00	0
10	14.76	0.073	14.79	0.062
15	14.75	0.075	14.79	0.062
20	14.77	0.070	14.66	0.103
25	14.74	0.077	14.43	0.170
30	14.71	0.086	14.54	0.138
40	14.75	0.075	14.48	0.155
50	14.74	0.077	14.43	0.170
60	14.76	0.071	14.48	0.155
90	14.77	0.069	14.54	0.139
120	14.76	0.071	14.43	0.170

Q: quantity of bound cations.

B.1.2 The individual binding

Time (min.)	Conc. of Ca (II) (ppm)	Q of Ca (II) (mg/g)	Conc. of Ni (II) (ppm)	Q of Ni (II) (mg/g)
0	15	0	15	0
5	14.45	0.165	14.18	0.246
10	14.45	0.165	14.10	0.270
15	14.29	0.212	14.01	0.297
20	14.14	0.259	13.91	0.330
25	14.19	0.243	13.99	0.302
30	14.03	0.290	13.95	0.315
40	14.19	0.243	13.91	0.327
50	14.14	0.259	13.88	0.337
60	14.40	0.181	14.08	0.276
90	14.19	0.243	14.21	0.238
120	14.29	0.212	13.96	0.313

Q: quantity of bound cations.

B.2 pH effect (Figure 3.15)

B.2.1 The competitive binding

pH	Conc. of Ca (II) (ppm)	Q of Ca (II) (mg/g)	Conc. of Ni (II) (ppm)	Q of Ni (II) (mg/g)
2	15.00	0	15.00	0
4	14.85	0.023	14.91	0.013
6	14.77	0.035	14.25	0.113
8	14.25	0.113	14.77	0.035
10	14.50	0.075	14.87	0.020
12	14.91	0.013	15.00	0

Q: quantity of bound cations.

B.2.2 The individual binding

pH	Conc. of Ca (II) (ppm)	Q of Ca (II) (mg/g)	Conc. of Ni (II) (ppm)	Q of Ni (II) (mg/g)
2	14.84	0.023	14.98	0.002
4	14.66	0.051	14.79	0.032
6	14.09	0.136	12.91	0.314
8	12.72	0.341	14.51	0.073
10	13.85	0.172	14.66	0.051
12	14.77	0.035	14.99	0.002

Q: quantity of bound cations.

B.3 Concentration effect (Figure 3.16)

B.3.1 The competitive binding

Conc. (ppm)	Conc. of Ca (II) (ppm)	Q of Ca (II) (mg/g)	Conc. of Ni (II) (ppm)	Q of Ni (II) (mg/g)
3	2.85	0.023	2.37	0.095
6	5.75	0.038	5.27	0.109
9	8.71	0.043	8.03	0.146
12	11.71	0.044	11.07	0.139
15	14.7	0.045	13.99	0.151
18	17.6	0.060	17.06	0.141
21	20.68	0.048	19.96	0.156
24	23.67	0.050	23.03	0.146
27	26.6	0.060	25.93	0.160
30	29.57	0.065	28.99	0.151

Q: quantity of bound cations.

B.3.2 The individual binding

Conc. (ppm)	Conc. of Ca (II) (ppm)	Q of Ca (II) (mg/g)	Conc. of Ni (II) (ppm)	Q of Ni (II) (mg/g)
3	2.54	0.069	1.73	0.190
6	5.24	0.114	4.51	0.224
9	8.14	0.129	7.29	0.256
12	11.12	0.132	10.13	0.281
15	13.99	0.152	12.91	0.314
18	16.8	0.180	16.12	0.282
21	19.84	0.174	18.92	0.312
24	22.91	0.163	22.05	0.292
27	25.8	0.180	24.87	0.320
30	28.7	0.195	27.99	0.302

Q: quantity of bound cations.